μSR and magnetism

ISIS muon training course

Stephen J. Blundell

Clarendon Laboratory, Department of Physics, University Of Oxford, UK

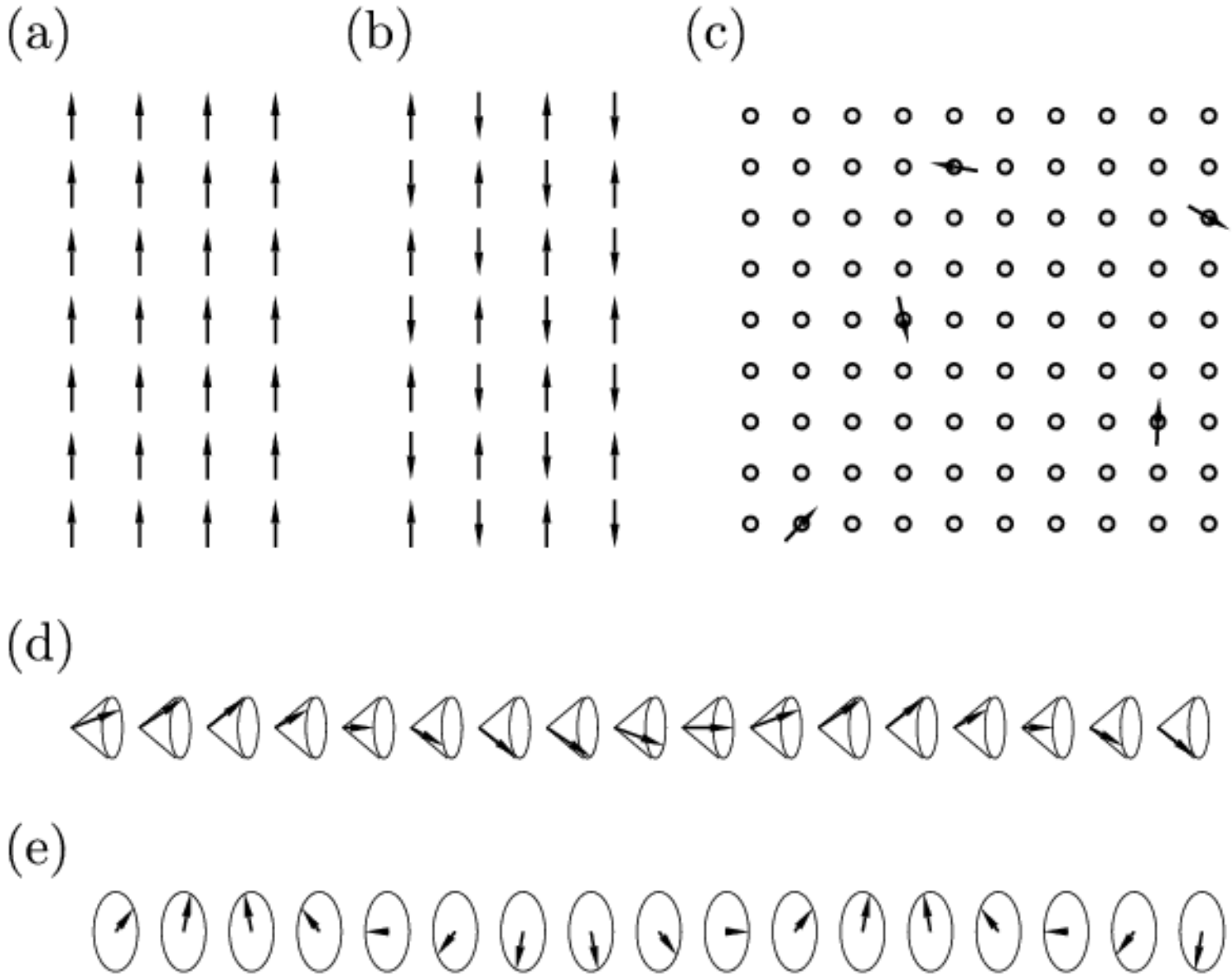
(a)
(b)
(c)
(d)
(e)

Muons as a probe of MAGNETISM

* microscopic probe : sensitive to short-range / local ordering
* can sense very weak effects
* works well in zero applied field

Muons as a probe of MAGNETISM

* μSR (muon-spin rotation) is particularly good for Small-moment magnetism, random magnetism and short-range effects
* can sense very broad-lines (up to ~100 MHz) and short relaxation times (down to ~10^{-8} s)

Muons as a probe of MAGNETISM

* one muon at a time

ultra-dilute limit!

* total # implanted muons << # atoms in solid

∴ low damage

In the presence of magnetic order, muons sense the internal magnetic field in a material, measured at the muon stopping site.

The muon spin precession frequency, $\omega_\mu = 2\pi\nu_\mu$, is given by

$$\omega_\mu = \gamma_\mu B_\mu .$$

This allows us to follow the temperature dependence of the magnetic order.

μSR data for an organic magnet

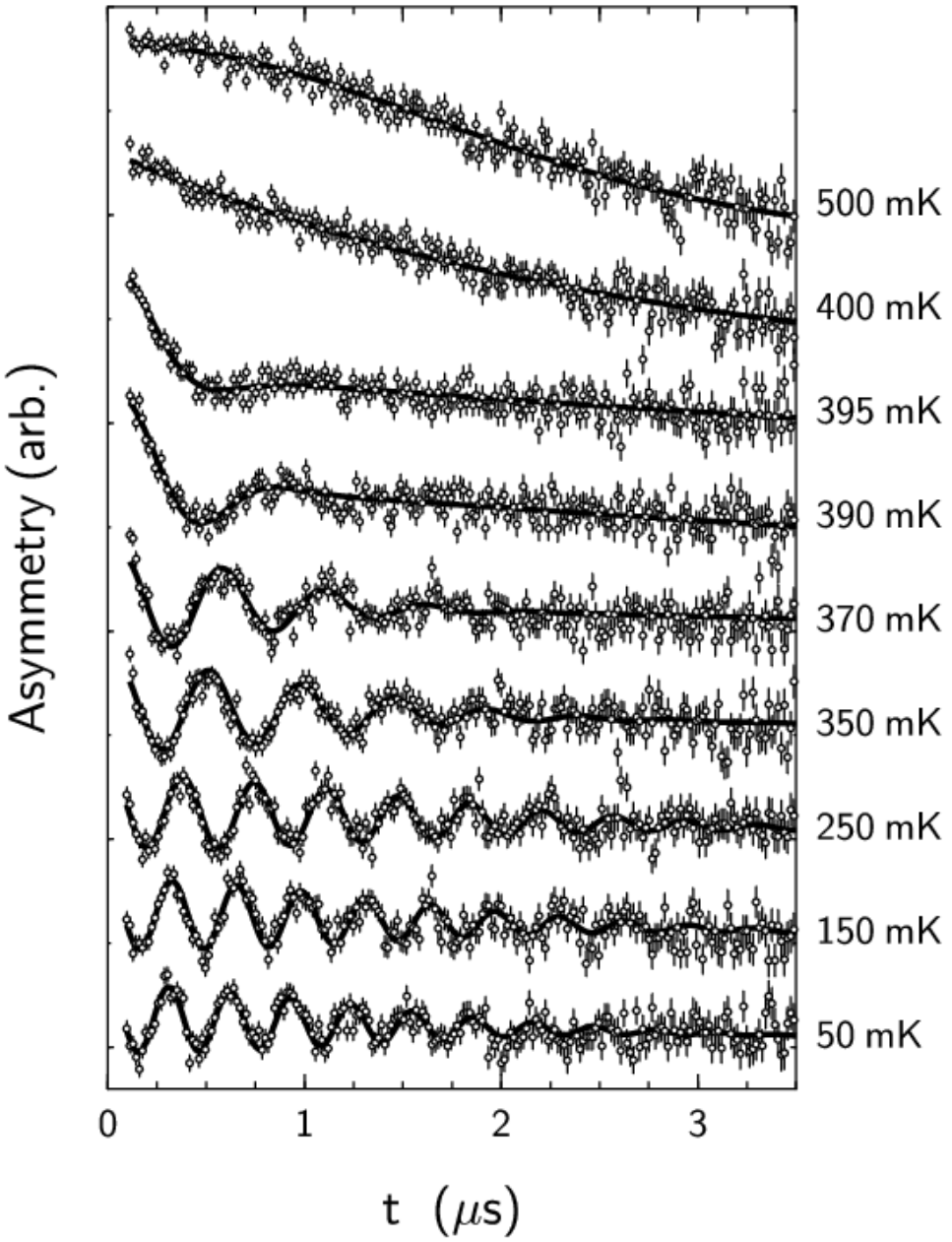

μSR and ordered organic ferromagnets and antiferromagnets

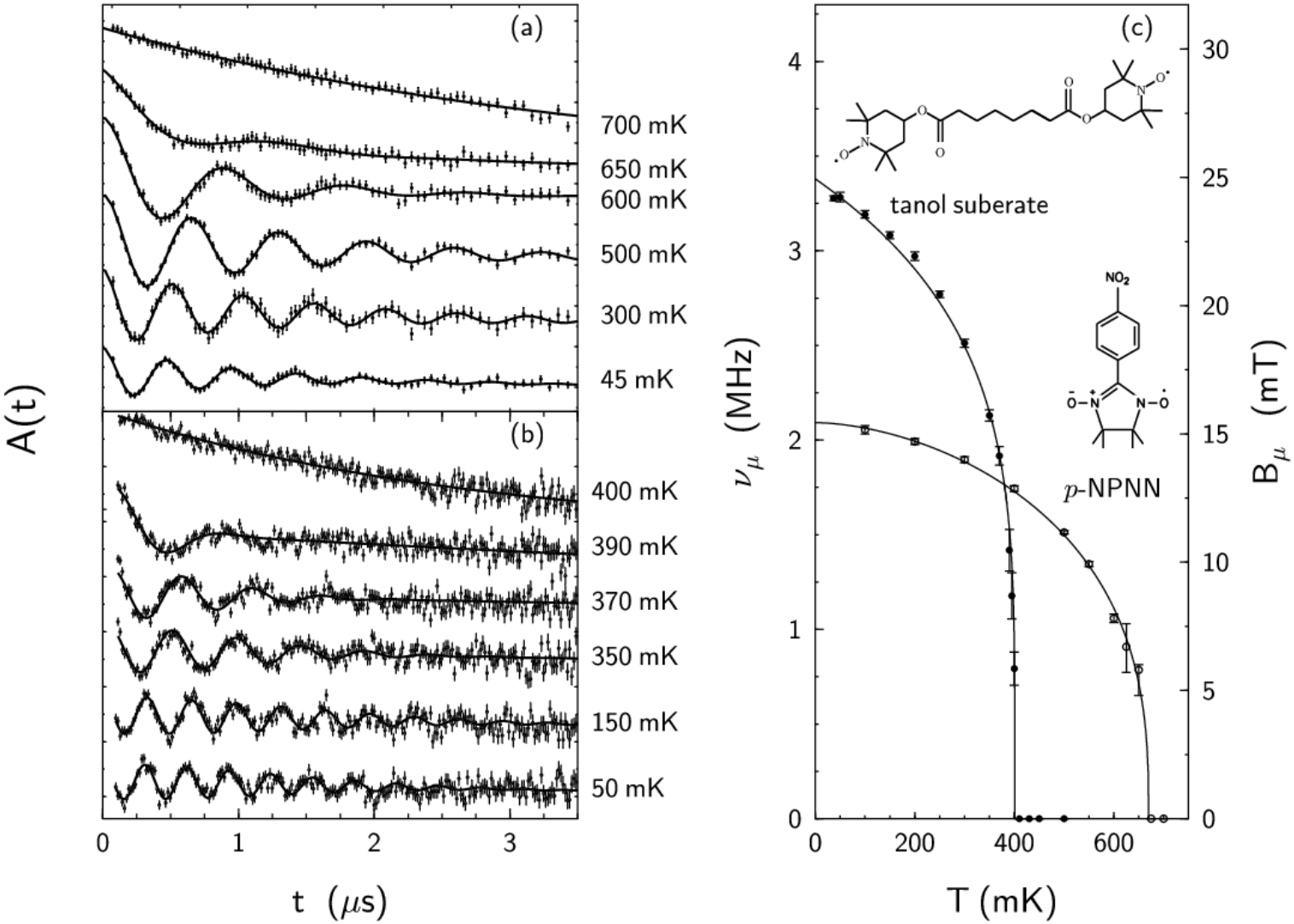

Uniformly weakly magnetic

Non-magnetic, with strongly magnetic impurities

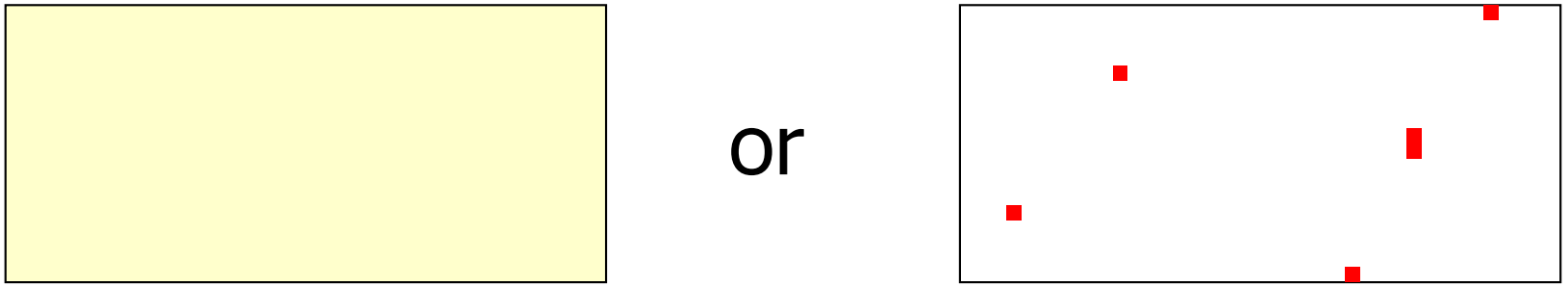

Susceptibility gives **average** information and therefore can give the same response for the situations sketched above (hence many false claims of room temperature organic ferromagnetism…)

μSR gives **local** information and therefore can distinguish between these two situations.

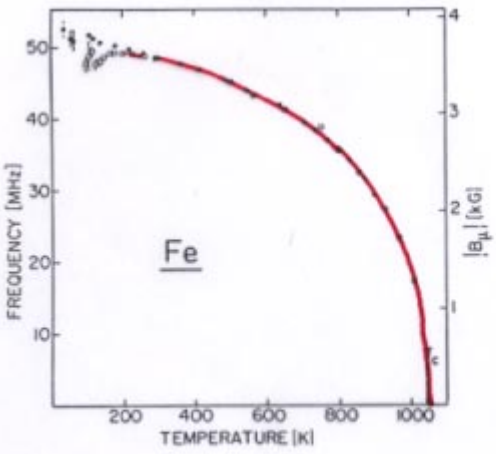

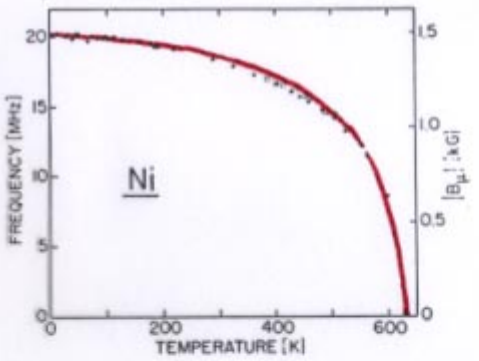

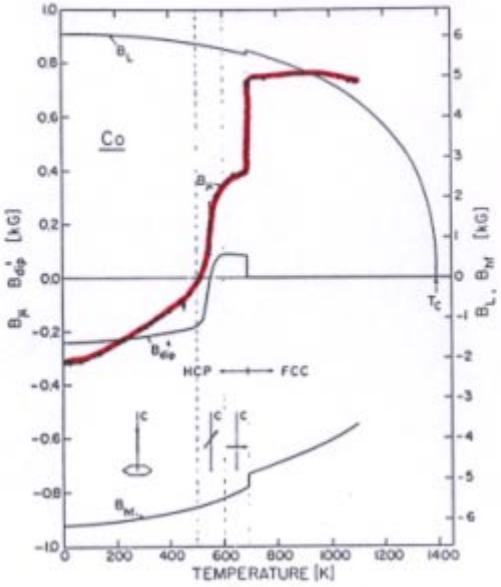

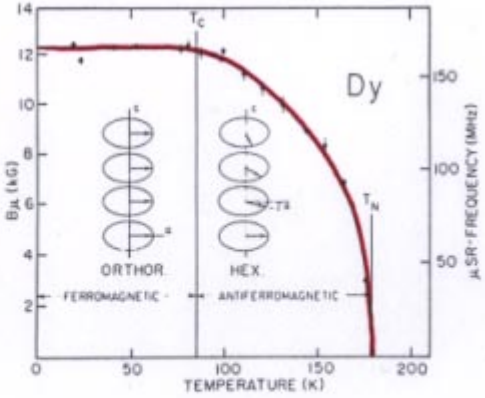

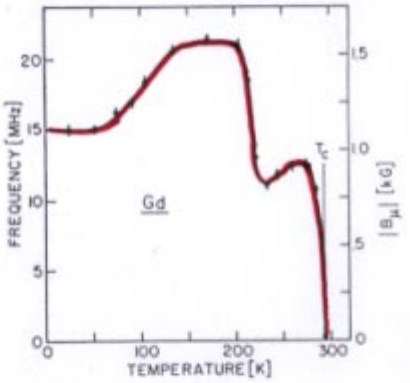

Positive muons as probes in ferromagnetic metals

A. B. Denison[a]), H. Graf[b]), W. Kündig and P. F. Meier
Physik-Institut der Universität Zürich, Zürich, Switzerland

Helv. Phys. Acta **52**, 460 (1979)

μ sits at highly symmetrical sites e.g. octahedral interstices

Antiferromagnets.

μSR works just as well with AFMs ∵ probes LOCAL fields

Example: MnO

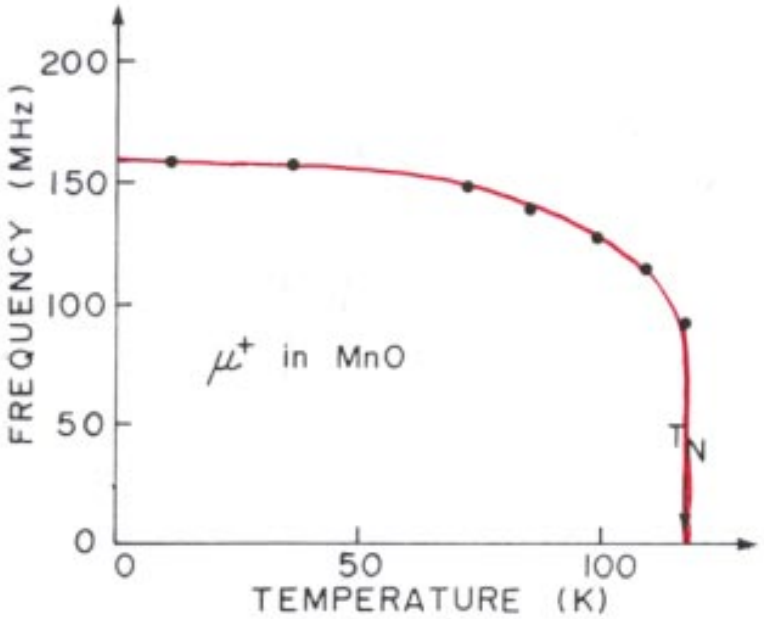

good spin precession signal (corresponds to 1.14 T at 0K, in ~ agreement with $S = 5/2$ dipolar field and hyperfine field).

Uemura et al Hyp. Int. 17, 339 (1984)

Muon-spin rotation

$$P_z(t) = \sum_i A_i \cos(\gamma_\mu |B_i| t)$$

- $P_z(t)$: muon-spin polarization
- i: muon-sites
- $|B_i|$: local magnetic field at muon-site

- Usually just one, or two, muon-sites but may need to take account of broadening / dynamics ...

e.g. $P_z(t) = \frac{1}{3} e^{-\lambda_\parallel t} + \frac{2}{3} e^{-\lambda_\perp t} \cos \omega_\mu t$

[polycrystalline] $\lambda_\parallel = 1/T_1$, $\lambda_\perp = 1/T_2$

- $|B_i| \propto M(T)$

$M(T)$: ORDER PARAMETER

AFM order in $LiVGe_2O_6$

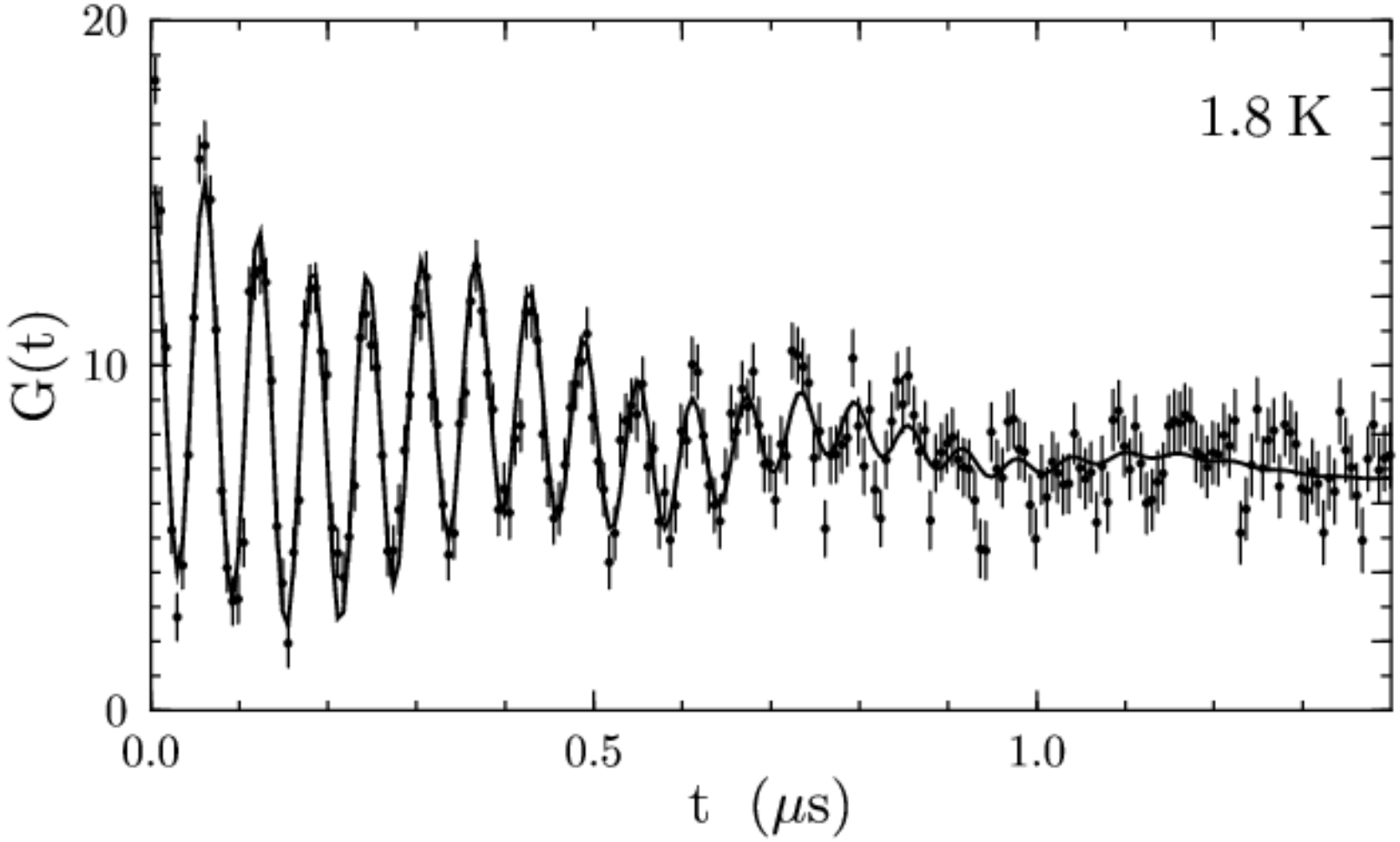

A hybrid molecular magnet

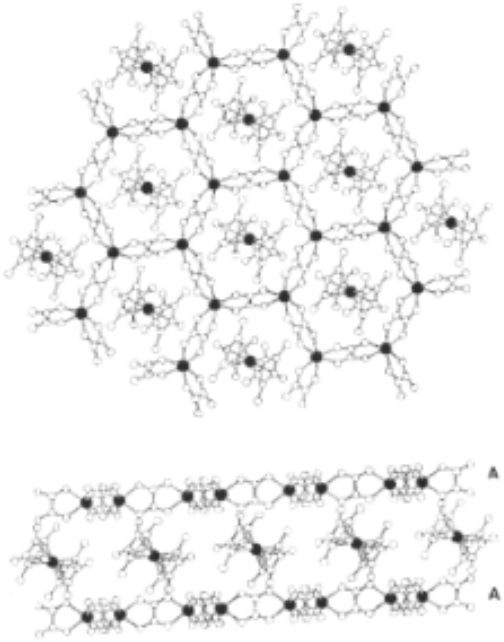

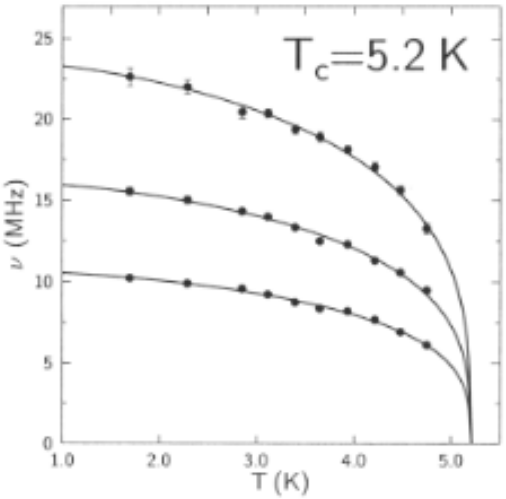

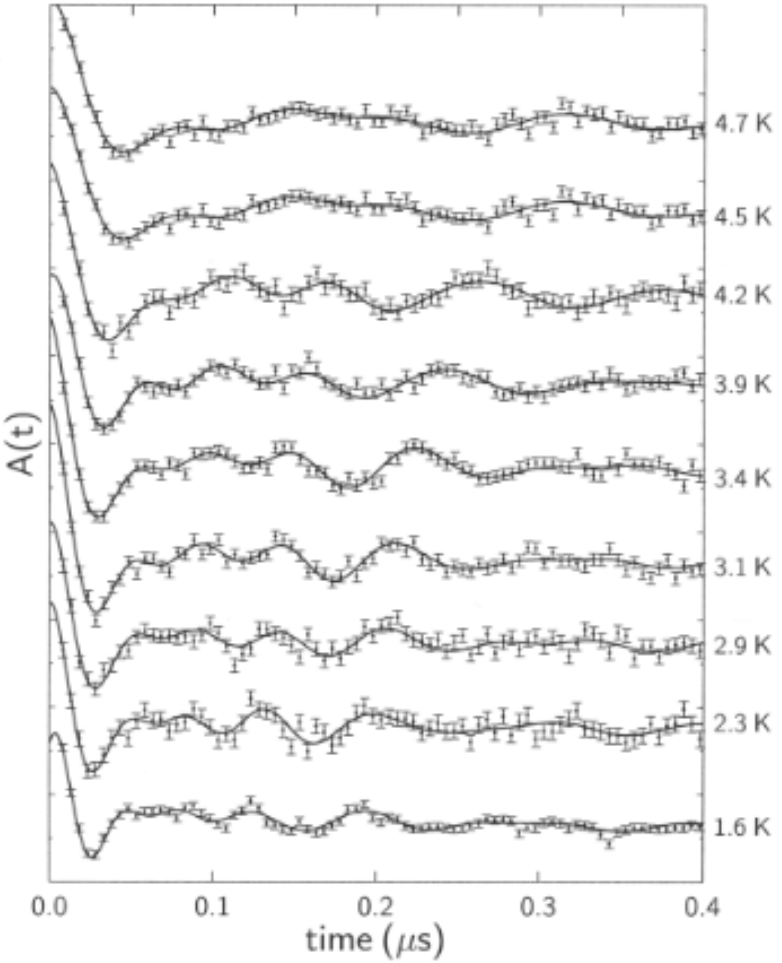

Local magnetic field at the muon site

* $B_L = \frac{\mu_0 M}{3}$ — LORENTZ FIELD
  site independent
  zero for antiferromagnets

* $B_{dip}(\underline{r}_\mu)$ — DIPOLAR FIELD
  depends on muon site
  depends on direction of $\underline{M}$

* $B_{hf}(\underline{r}_\mu)$ — HYPERFINE FIELD
  due to electron spin density at muon site

* B_{demag} — DEMAGNETIZATION FIELD
  depends on sample shape or domain structure

Dipole-dipole field

$$\underline{B}_{dip}(\underline{r}) = \frac{\mu_0}{4\pi} \sum_i \frac{1}{r_i^3} \left[\frac{3(\underline{m}_i \cdot \underline{r}_i)\underline{r}_i}{r_i^2} - \underline{m}_i \right]$$

Dipole-dipole field

$$B_{dip}(\underline{r}) = \frac{\mu_0}{4\pi} \sum_i \frac{1}{r_i^3} \left[\frac{3(\underline{m}_i \cdot \underline{r}_i)\underline{r}_i}{r_i^2} - \underline{m}_i \right]$$

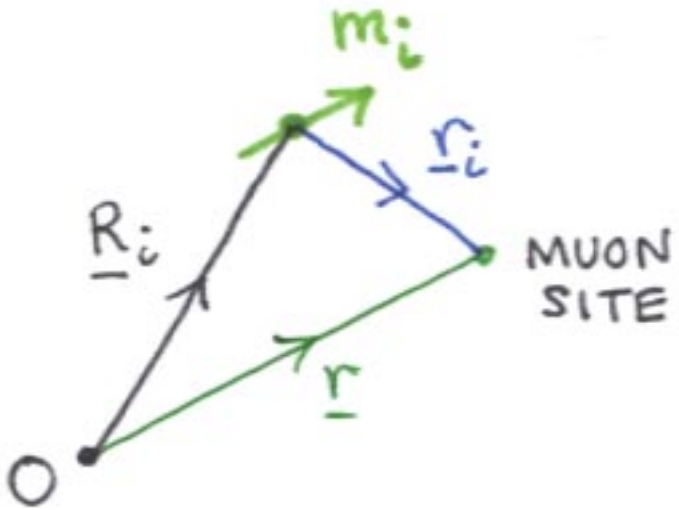

Dipole-dipole field

$$\underline{B}_{dip}(\underline{r}) = \frac{\mu_0}{4\pi} \sum_i \frac{1}{r_i^3} \left[\frac{3(\underline{m}_i \cdot \underline{r}_i)\underline{r}_i}{r_i^2} - \underline{m}_i \right]$$

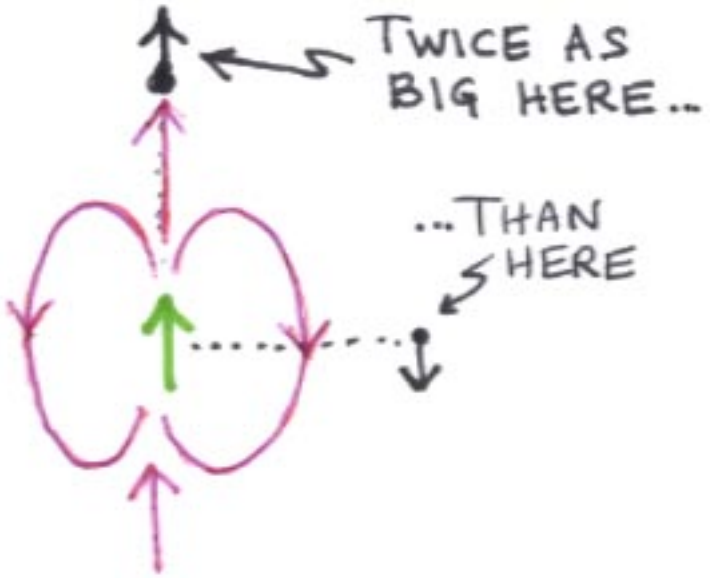

Dipole-dipole field

$$B_{dip}(\underline{r}) = \frac{\mu_0}{4\pi} \sum_i \frac{1}{r_i^3} \left[\frac{3(\underline{m}_i \cdot \underline{r}_i)\underline{r}_i}{r_i^2} - m_i \right]$$

Problem:

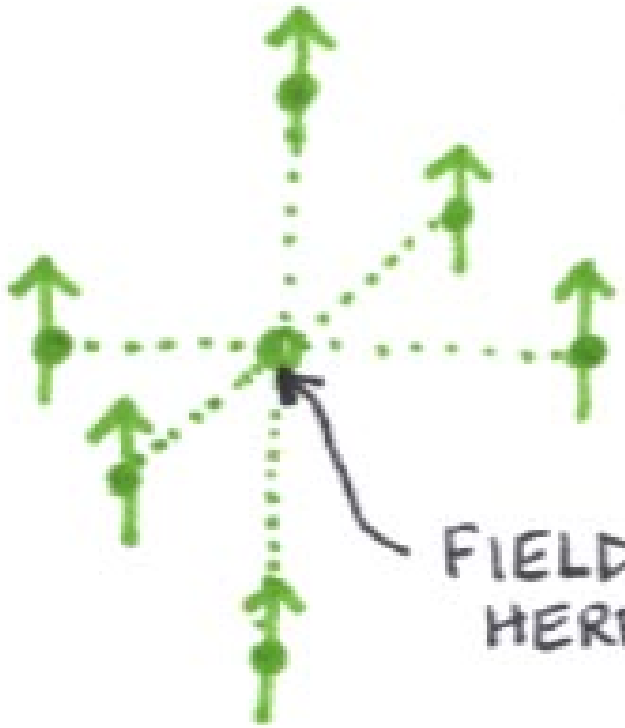

Dipolar fields

Dipolar field calculations:

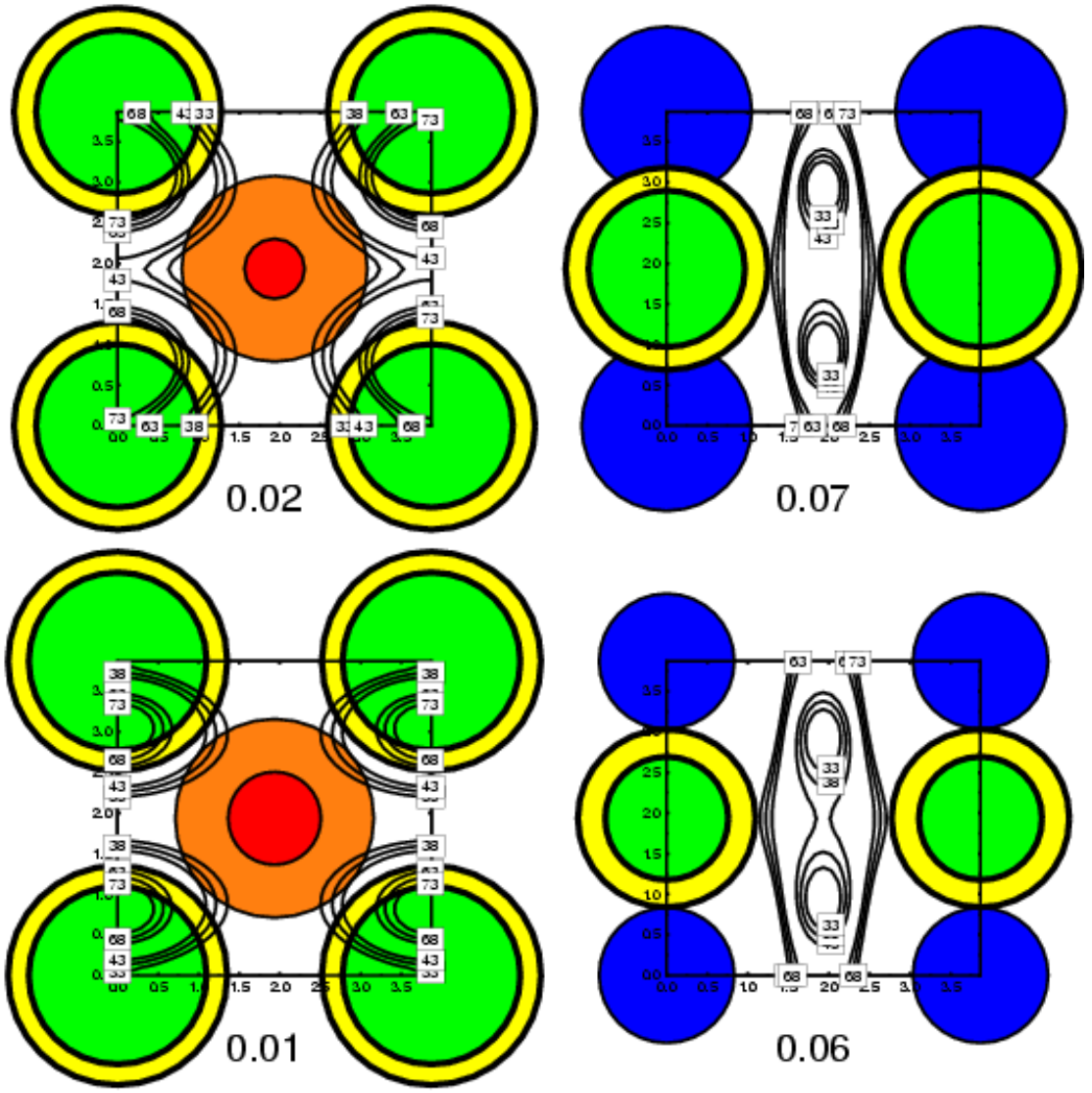

Antiferromagnetic ordering in $La_{2-x}Sr_xCuO_4$

neutrons were used to show La_2CuO_4 AFM with $T_N \sim 250\,K$

but $T_N(x)$ $x>0$ first explored with μ^+SR because less demanding with sample-size.

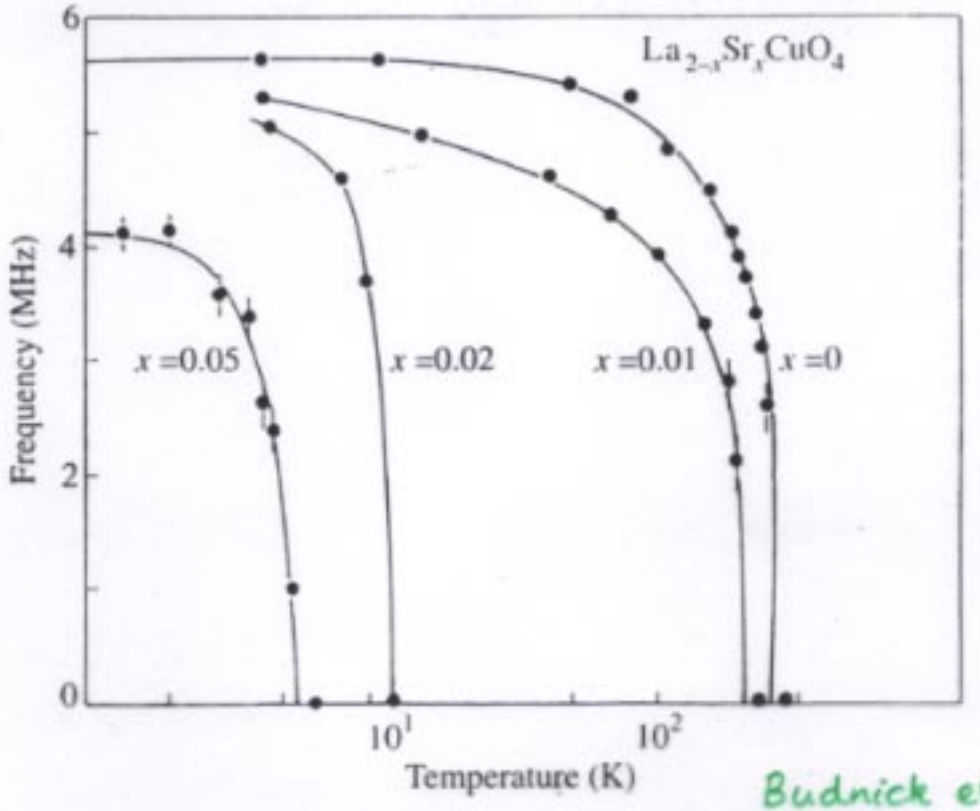

Budnick et al '88

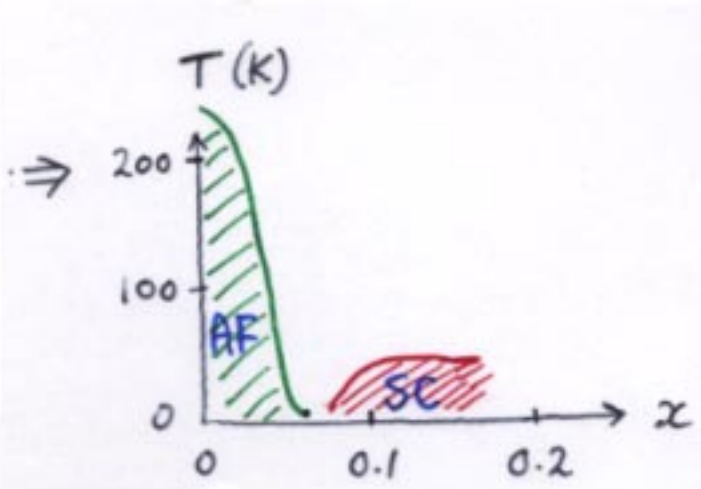

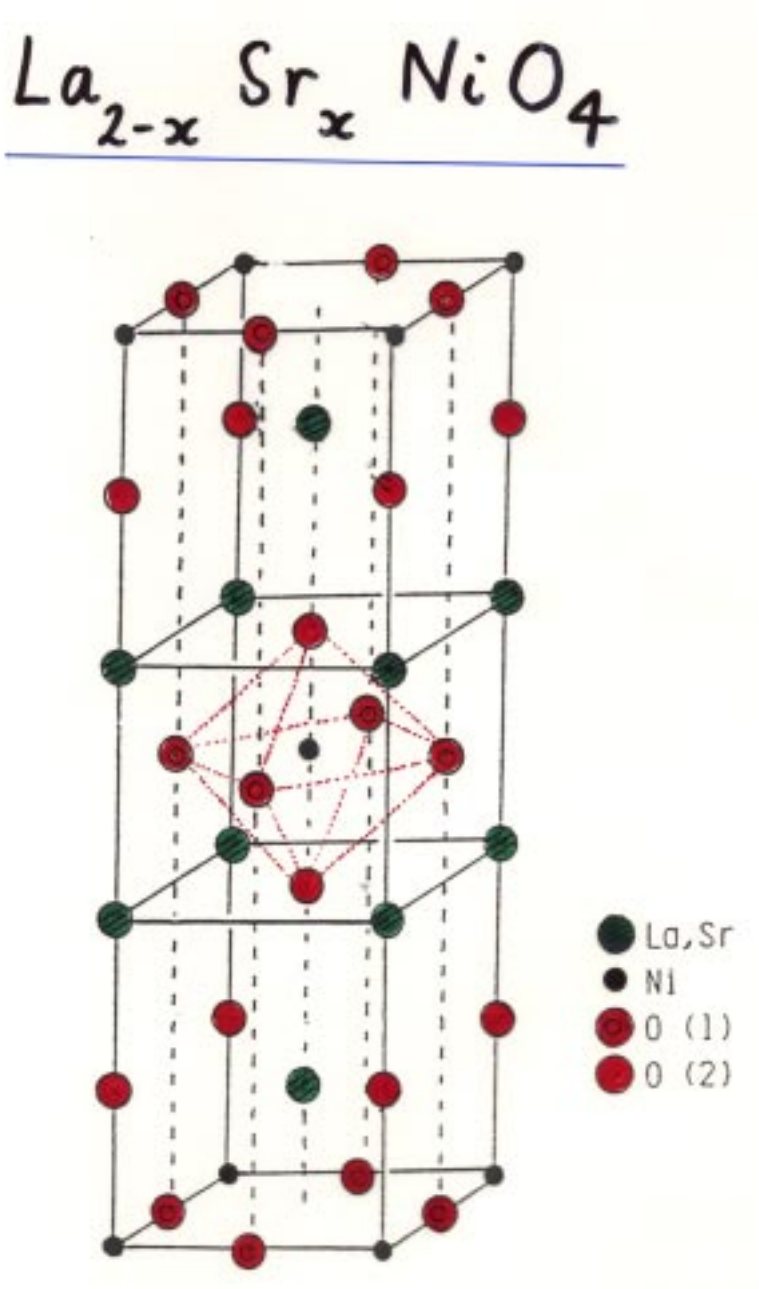

For cuprates, kill AFM with a few % of dopant and achieve maximum superconductivity at x~0.15. The normal state is a (weird) metal.

For these nickelates, only metallic at x~1.
No superconductivity.
Evidence for 2D ordered array of holes below ~230 K.

mSR used to find ground state for 0<x<1.

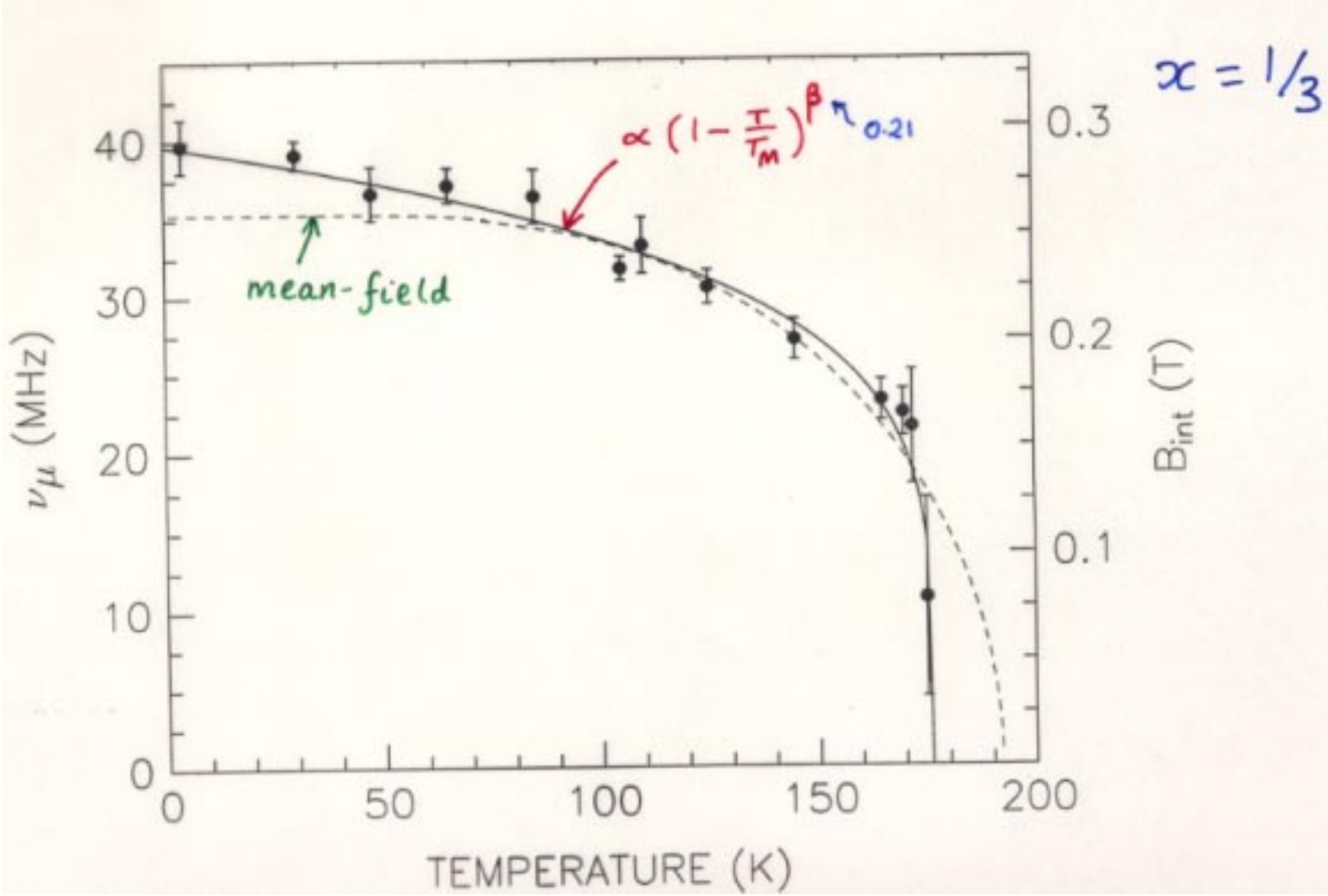

PRB **59** 3775 (1999)

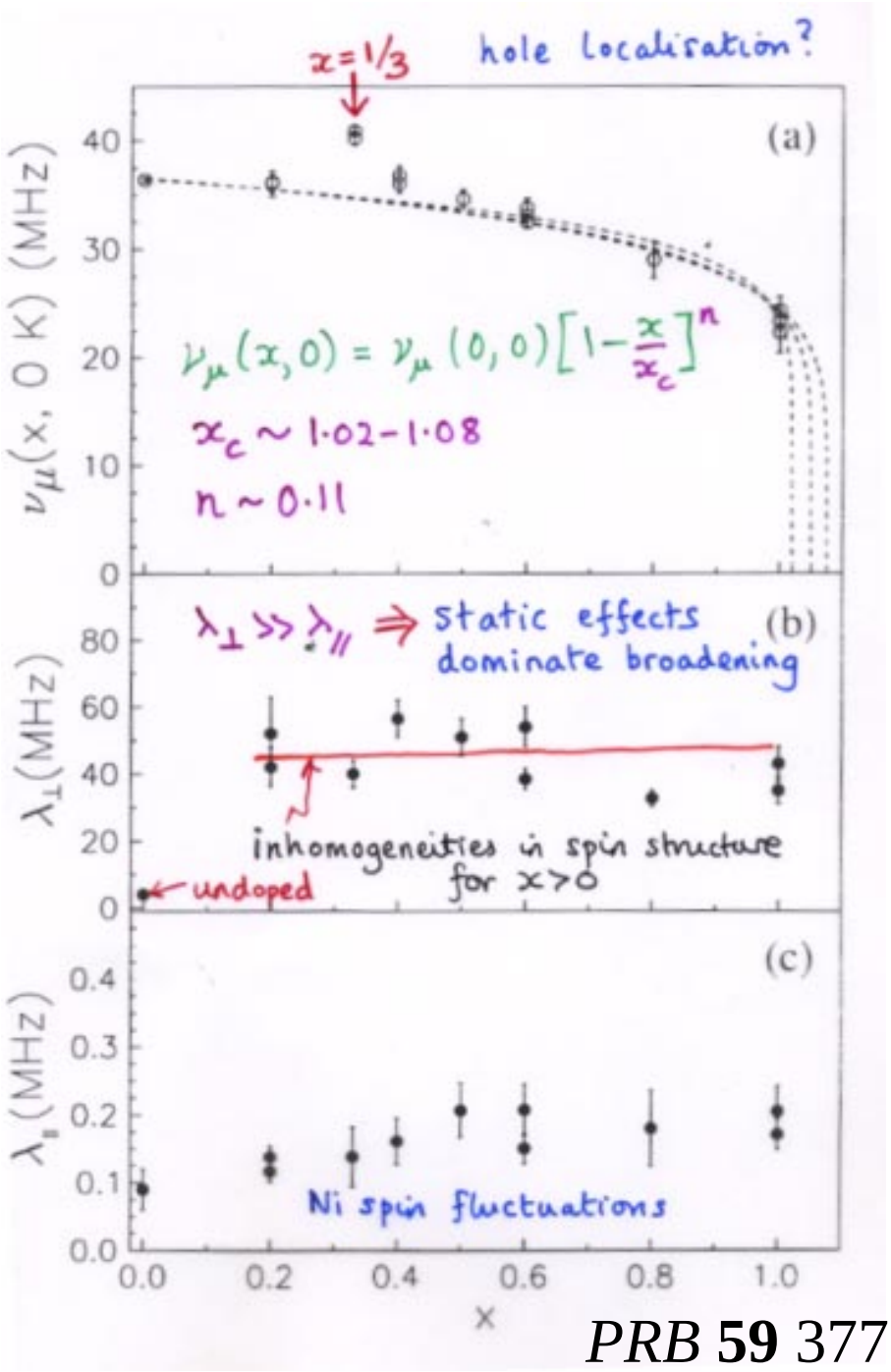

$\Rightarrow$ Phase diagram: $La_{2-x}Sr_xNiO_{4+\delta}$

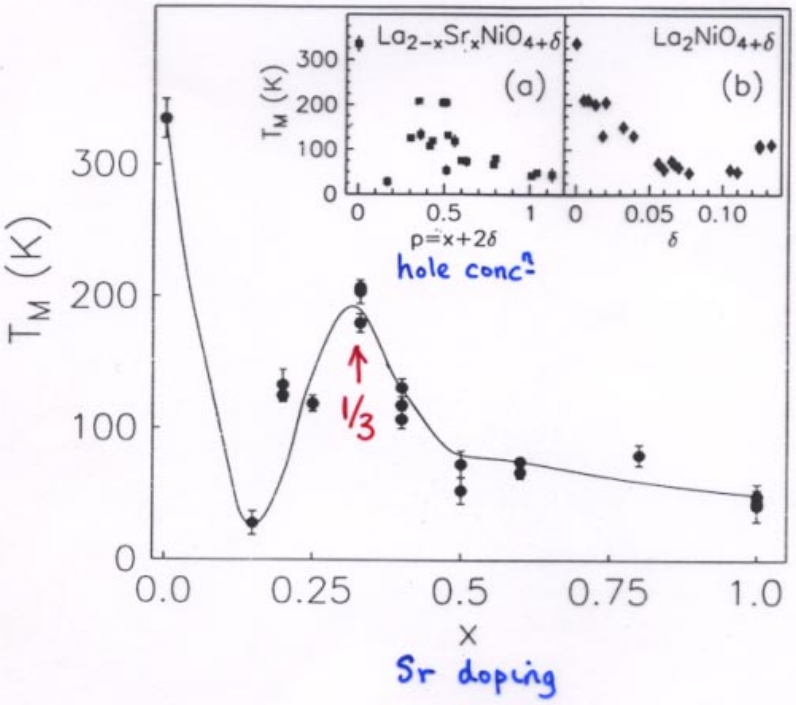

- different structural consequences of Sr doping and O doping
- stabilisation of $x = 1/3$ magnetic state

NB charge ordering $(\pm\varepsilon, \pm\varepsilon)$
spin ordering $(\frac{1}{2}\pm\frac{\varepsilon}{2}, \frac{1}{2}\pm\frac{\varepsilon}{2})$
$\varepsilon \sim$ hole doping coincide when $\varepsilon \sim 1/3$

PRB **59** 3775 (1999)

Bilayer manganates

(important for colossal magnetoresistance)

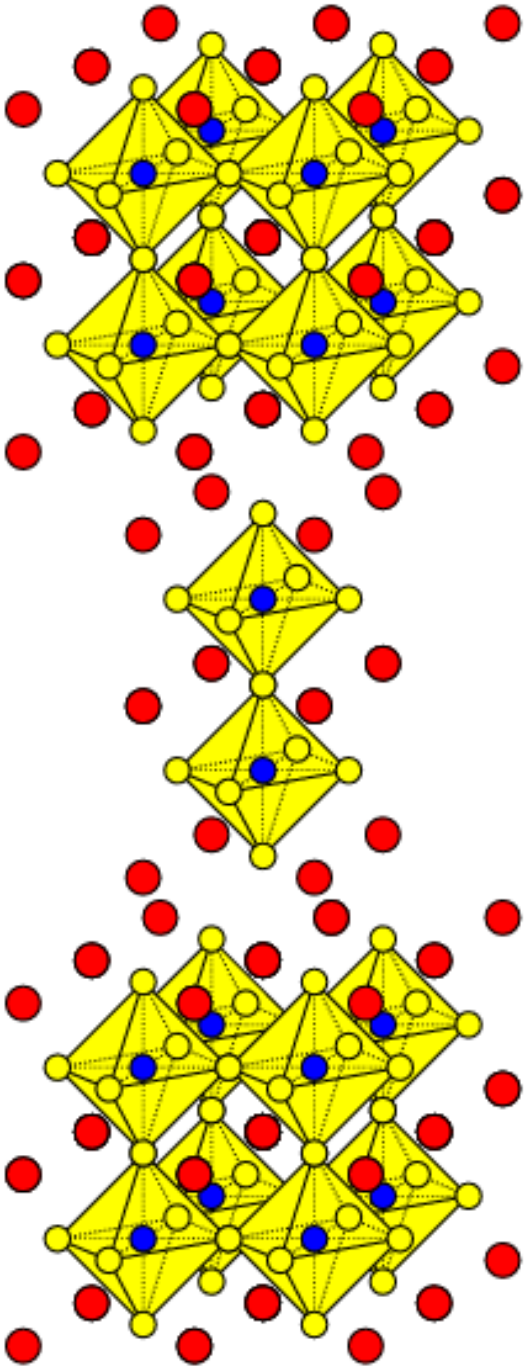

Bilayer manganates

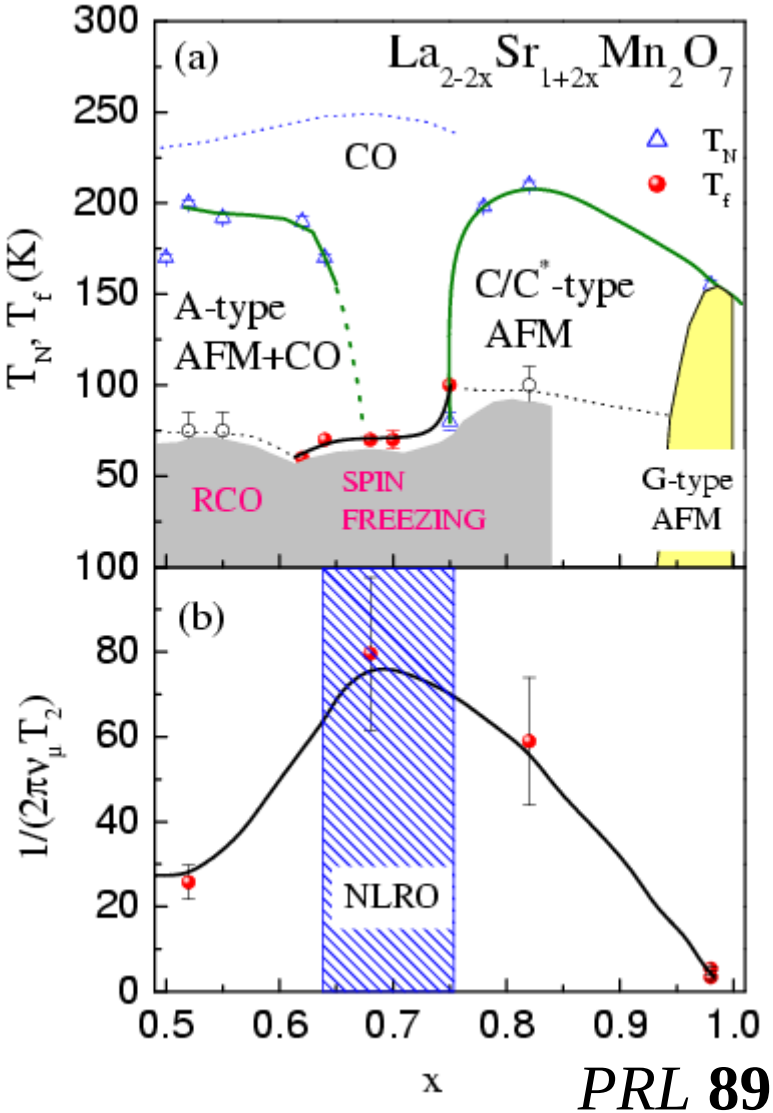

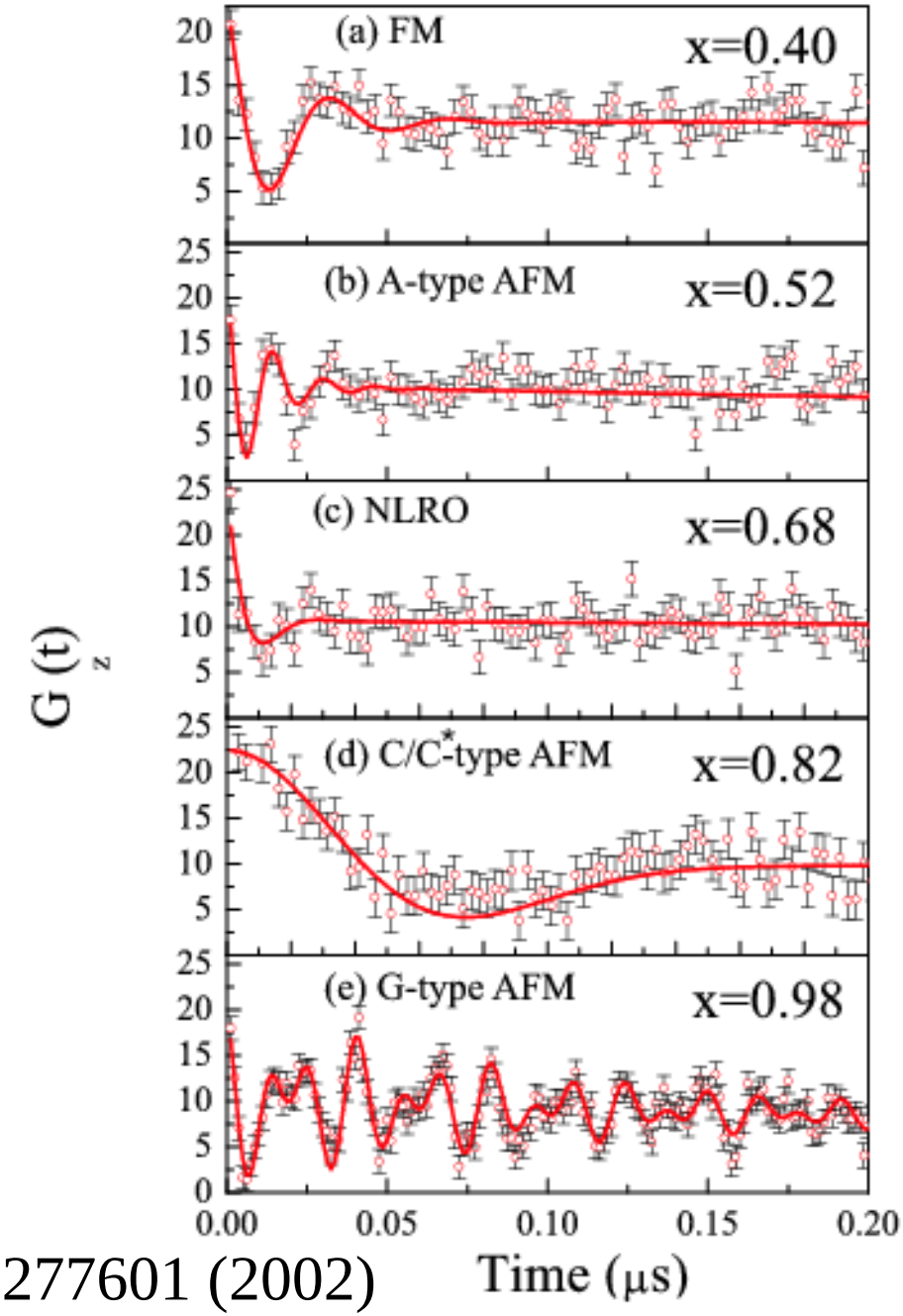

PRL **89** 277601 (2002)

Low-dimensional magnetism

D is the dimension of the order parameter

d is the dimension of the lattice

	$D = 1$ Ising	$D = 2$ XY	$D = 3$ Heisenberg
$d = 1$	no order	no order	no order
$d = 2$	order	order	no order
$d = 3$	order	order	order

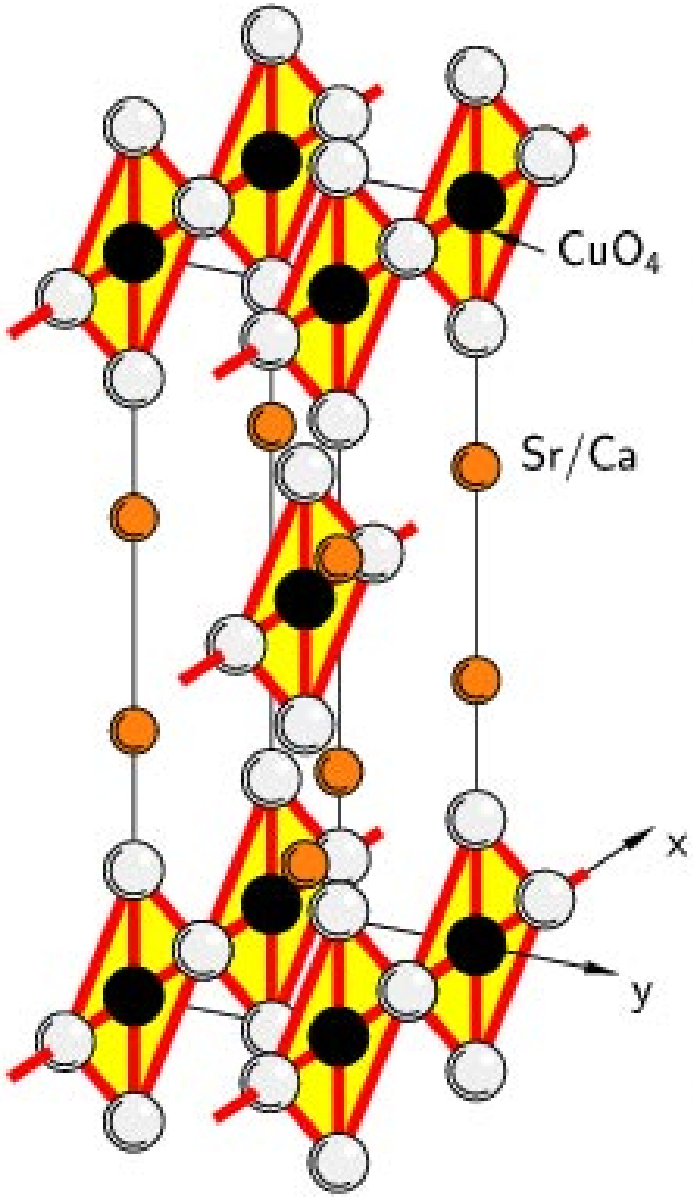

Sr_2CuO_3

Chains of
-Cu-O-Cu-O-Cu-O-Cu-
along x-axis

superexchange through oxygen anions

chains well separated and J'/J small

Muon data

Sr_2CuO_3

Ca_2CuO_3

Kojima et al
PRL **78** 1787 1997

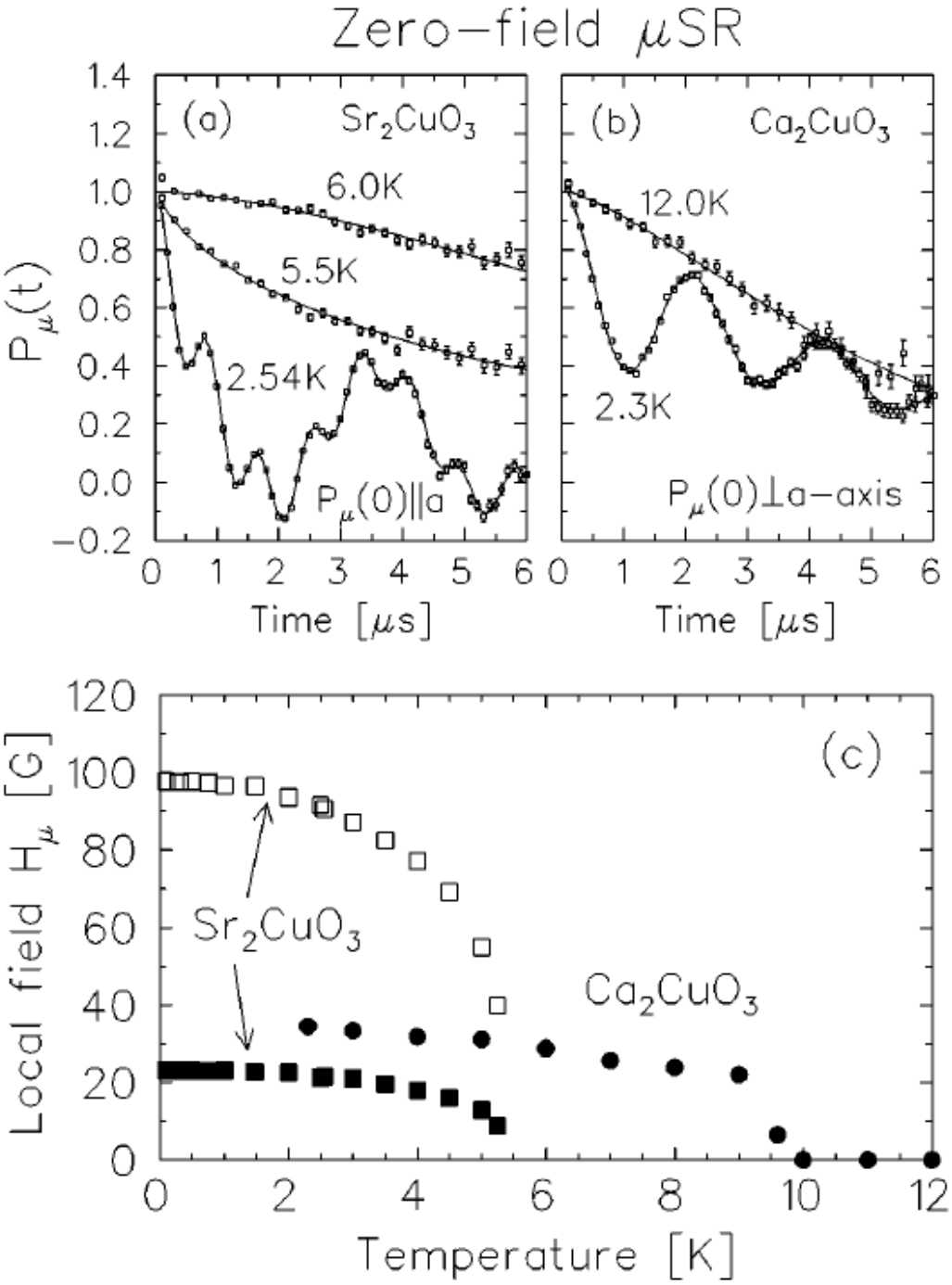

Muon data

$LaSrCoO_3H_{0.7}$

Our data:
Science **295** 1882 2002

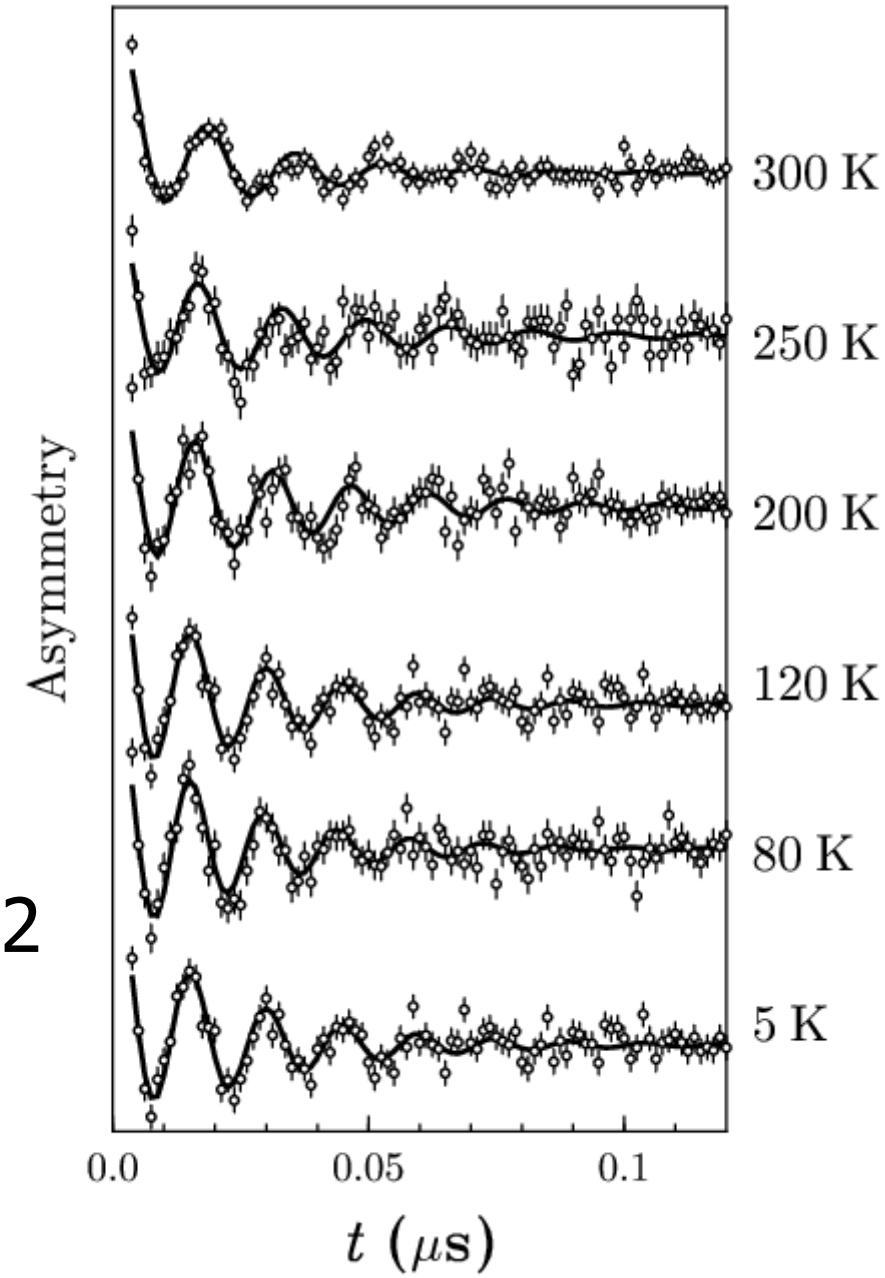

Muon data

The internal magnetic field is very high (~0.5 T) which is much greater than in Sr_2CuO_3 (~0.01 T)

T_N is well above room T in our compound, much greater than ~5 K in Sr_2CuO_3 and ~10 K in Ca_2CuO_3

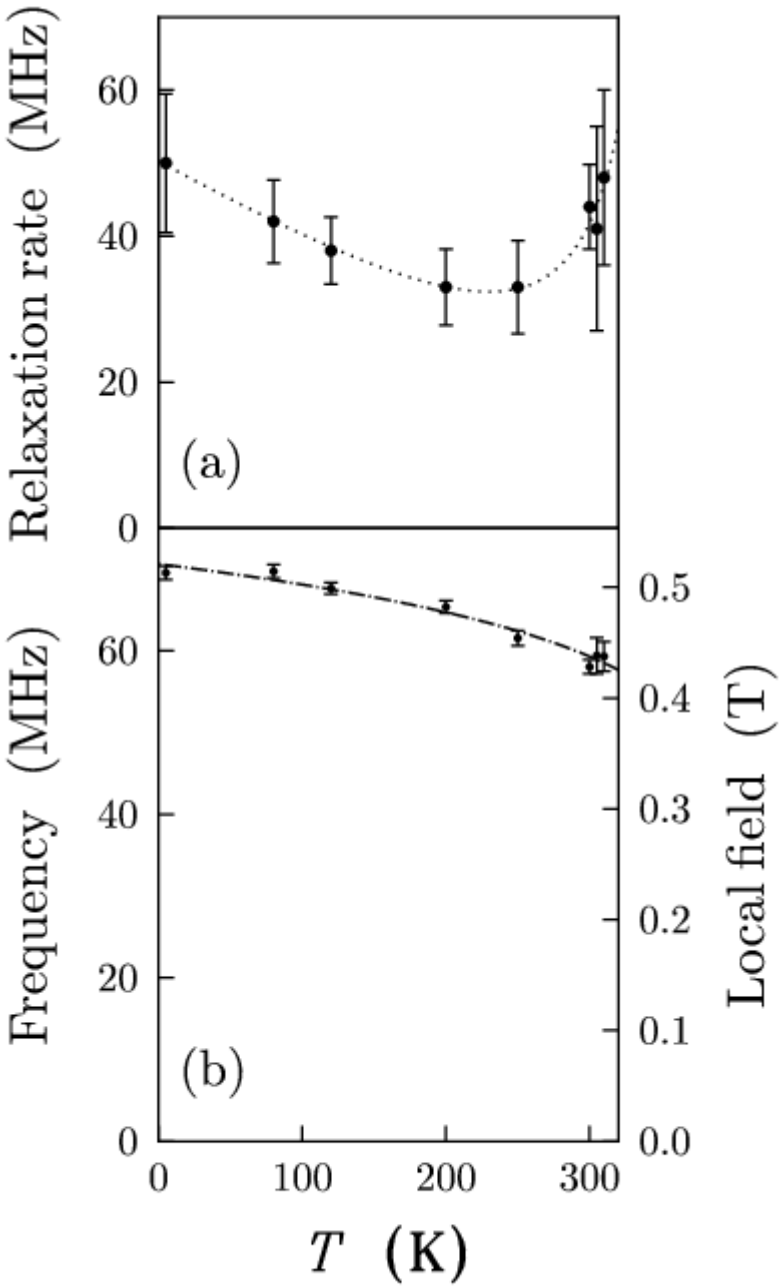

Synthesis of new spin chain

Attempt to separate the chains further:
Start with $LaSrCoO_4$ which has a K_2NiF_4 structure
(Co is Co^{III}, $3d^6$, S=2)

This is reduced using CaH_2 at 450°C to produce a new phase which resembles Sr_2CuO_3 in crystal structure

suspect $LaSrCoO_3$ (here Co is Co^{I}, $3d^8$, S=1)

the chains are further separated (0.360 nm) in this compound than in Sr_2CuO_3 (0.349 nm) or Ca_2CuO_3 (0.325 nm)

Conclusion:

$LaSrCoO_3H_{0.7}$ contains the hydride ion

H^- $(1s^2)$

Hydride ions can transmit exchange interactions very effectively! This leads to the separated chains being bridged, raising the transition temperature of our compound to well above room temperature!

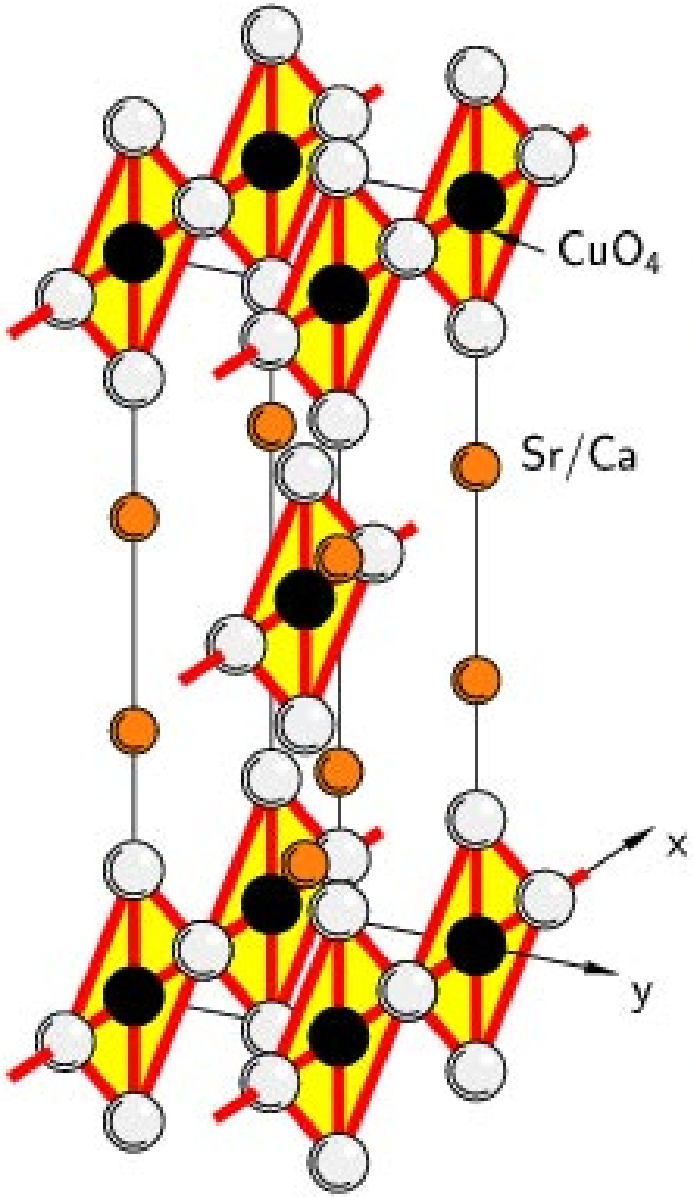

Sr_2CuO_3

Chains of
-Cu-O-Cu-O-Cu-O-Cu-
along x-axis

superexchange through oxygen anions

chains well separated and J'/J small

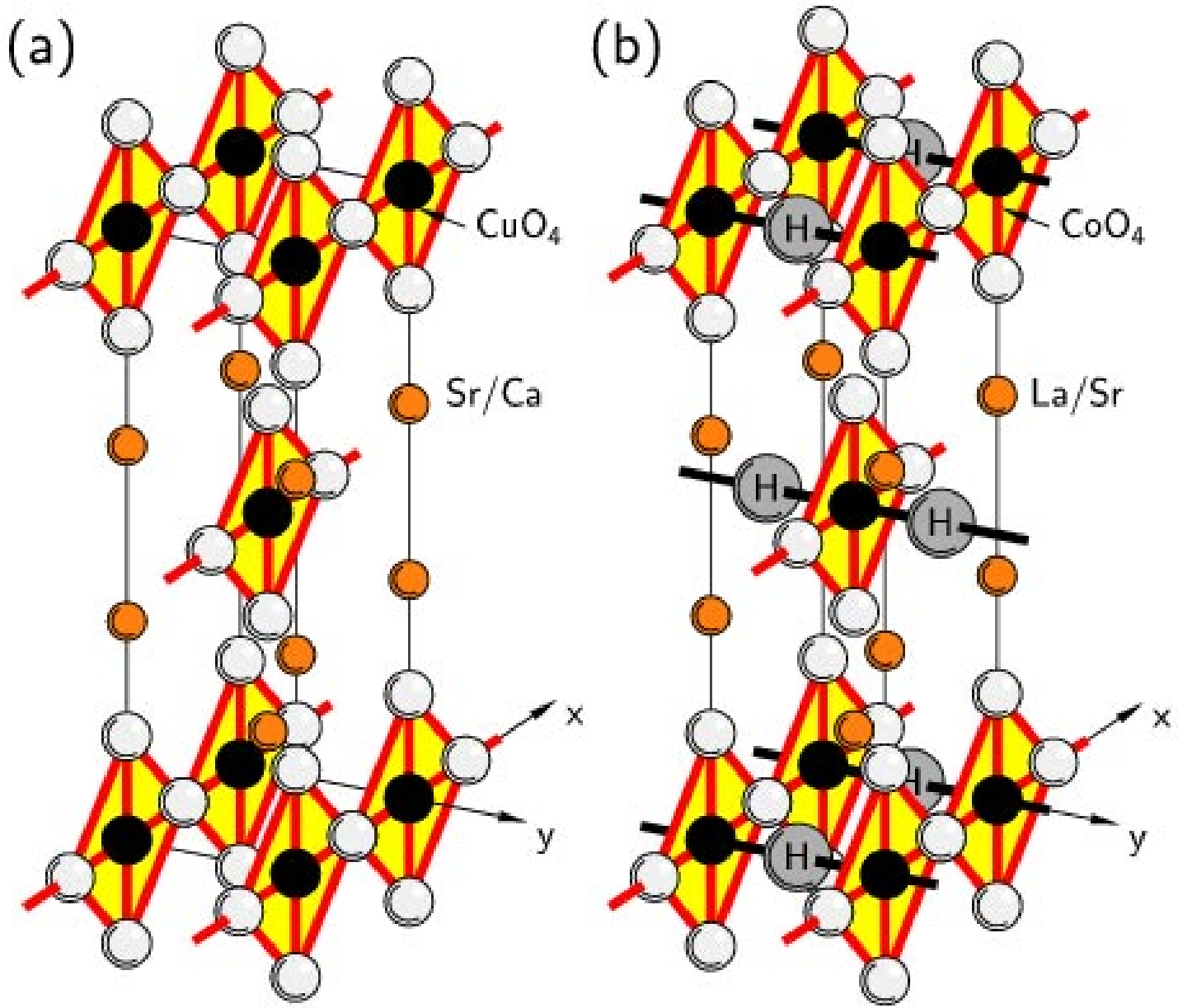
(a)
CuO_4
Sr/Ca
x
y
(b)
H
H
H
H
H
CoO_4
La/Sr
x
y

AF order from neutron diffraction

Spin structure deduced from powder neutron diffraction at 300 K.

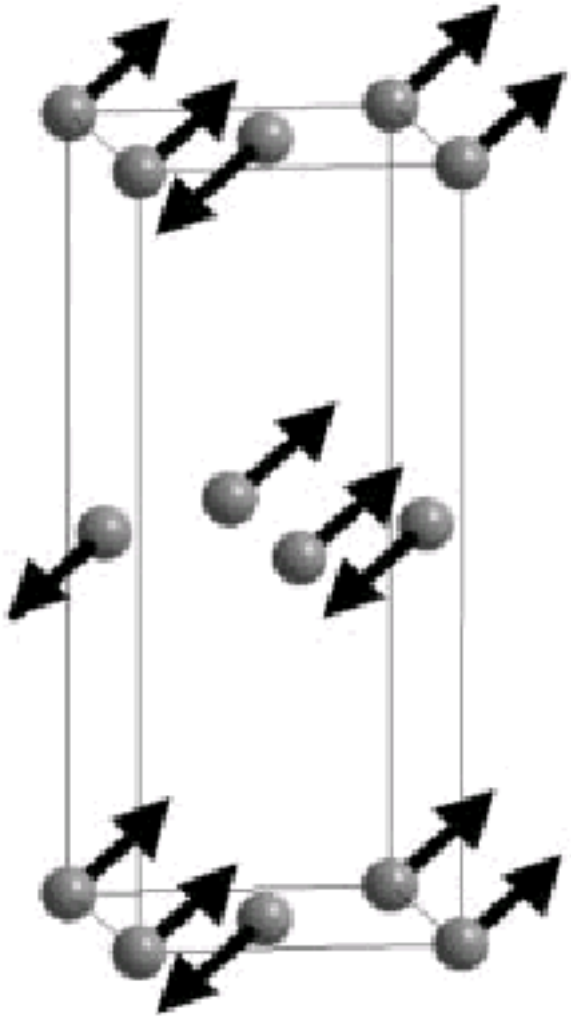

Discussion

Hydride ion can engage in strong covalent bonding with transition metal centres in molecular species

Co-H distance is 0.18 nm, shorter than either Co-O distances. Strong covalency expected for Co^{2+} and H^- implies effective AF coupling

Note that $LaSrCoO_{3.5}$ has T_N=110 K, with a similar concentration of bridging ions in the *ab* plane, demonstrating the efficiency of hydride superexchange

BEDT-TTF molecule

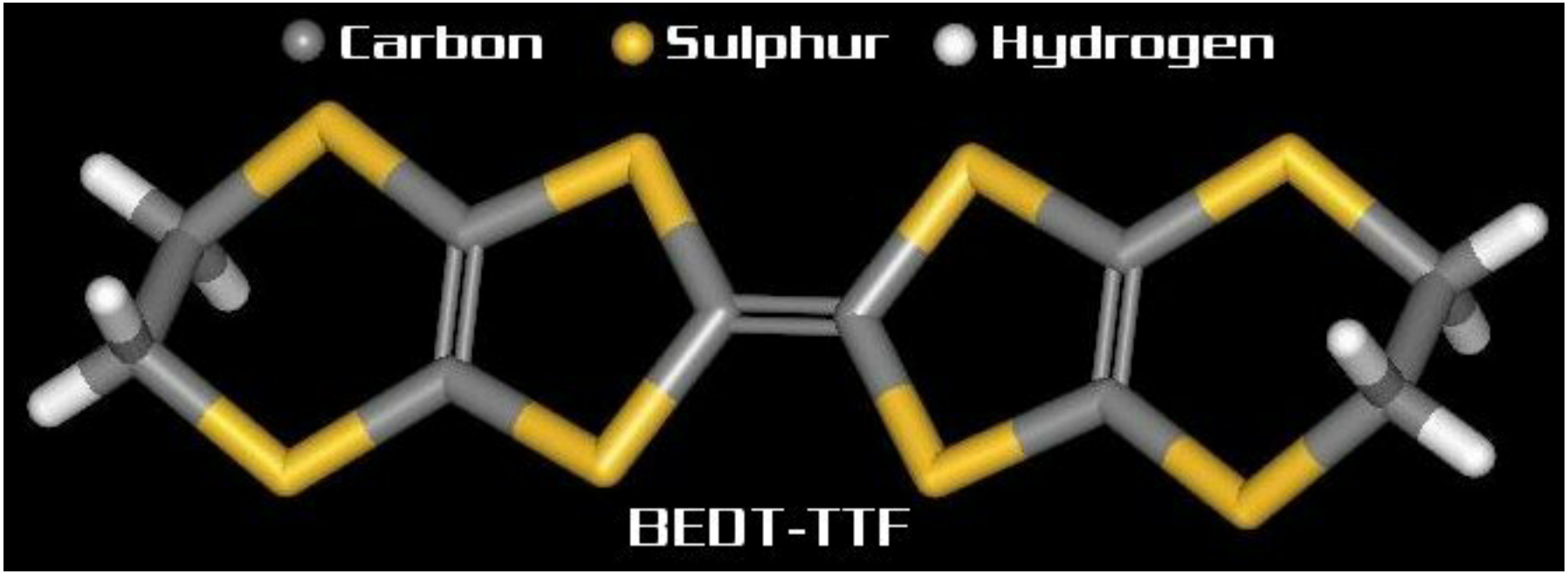

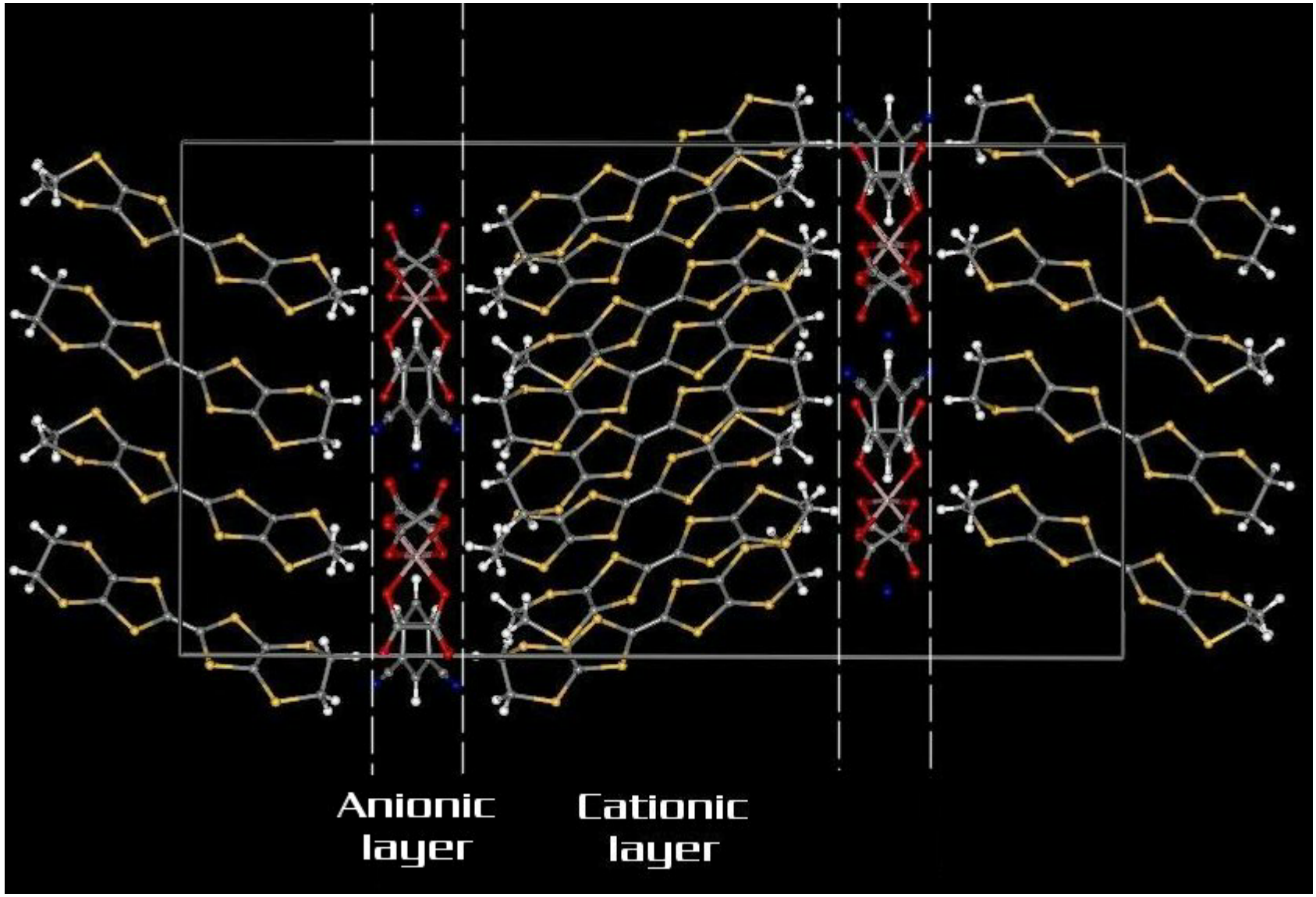
Anionic
layer
Cationic
layer

Site close to the $FeCl_4$ plane.

Site nearthe centre of a BETS molecule (perhaps through muonium addition to a C=C bond.

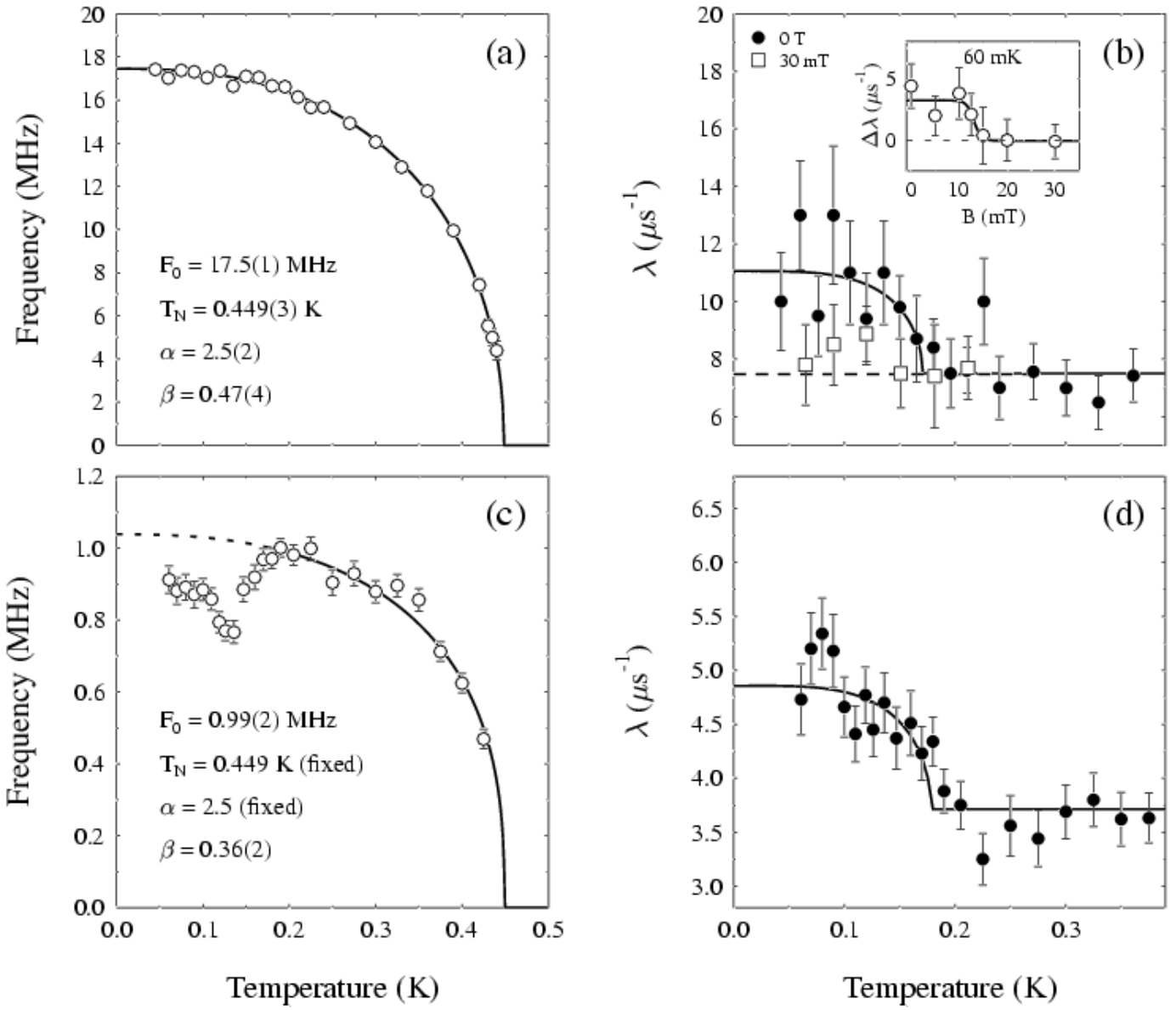

F.L. Pratt et al Synth. Met. in press

TMTSF salts

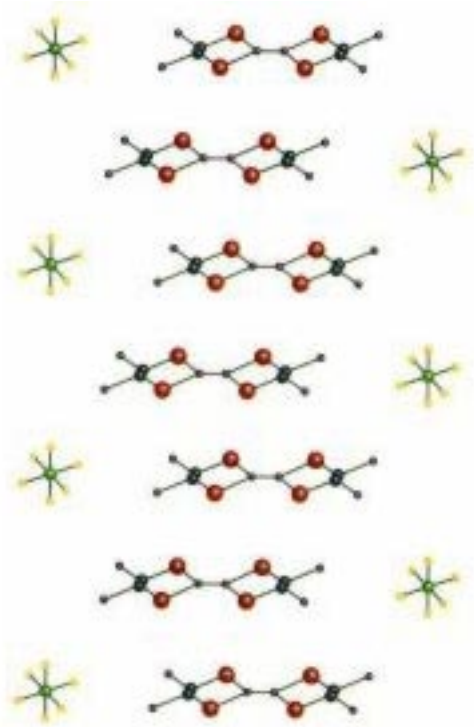

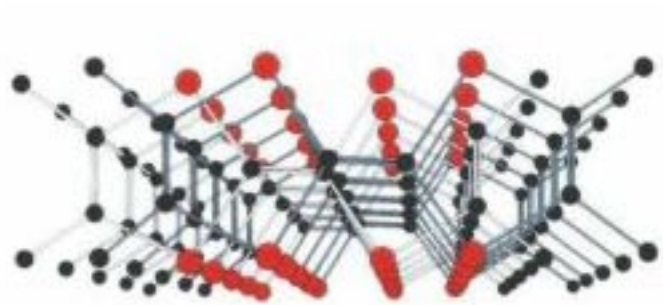

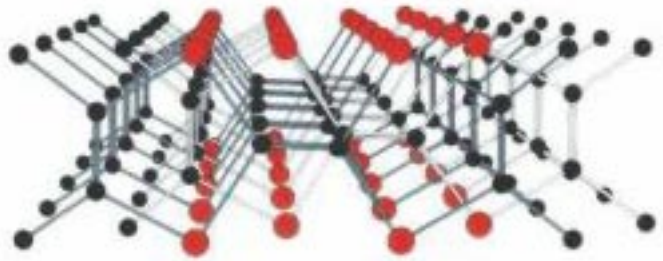

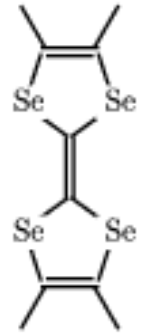

TMTSF

Stacks of TMTSF molecules ⇒ 1D chains

TMTSF salts

Very rich
phase diagram

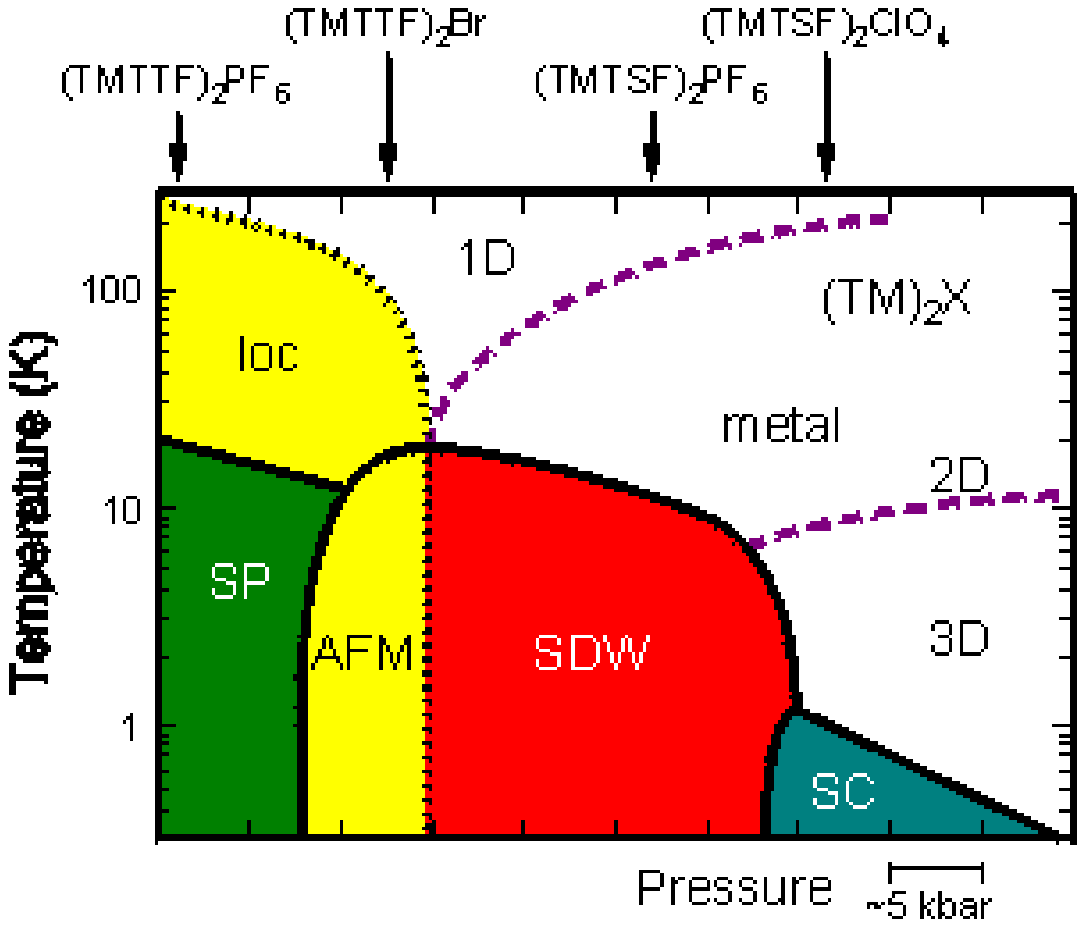

1D electron gas unstable to SDW formation

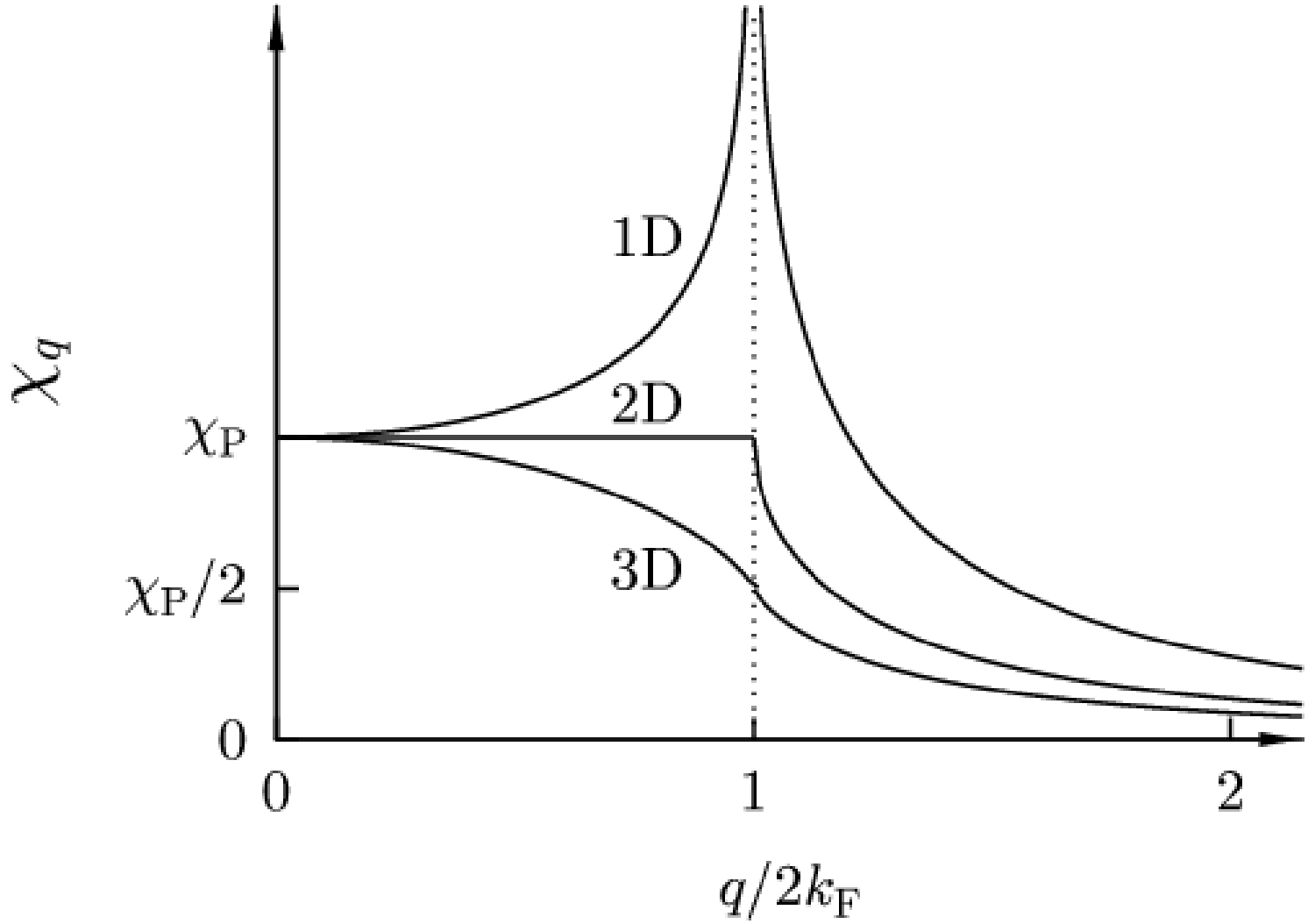

Spin-density wave

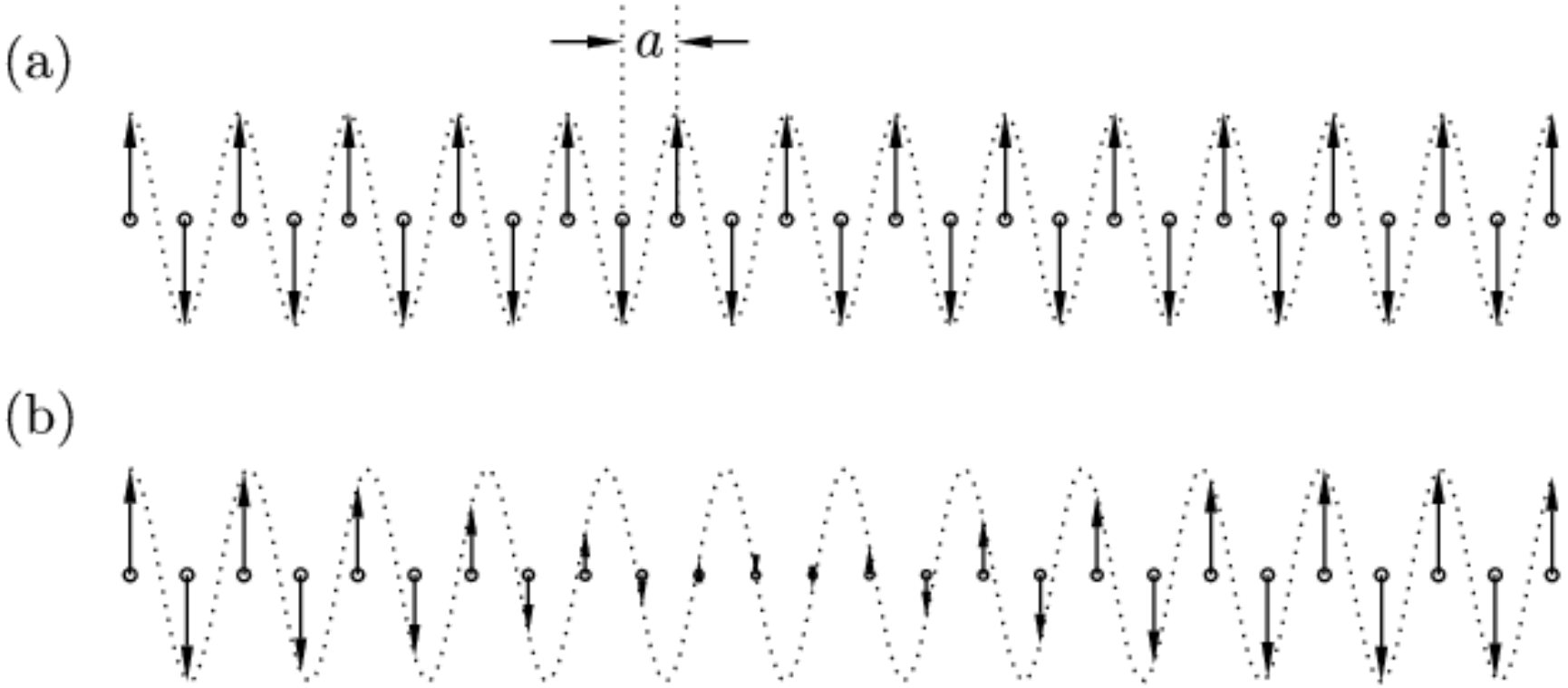

Raw muon data on $TMTSF_2X$

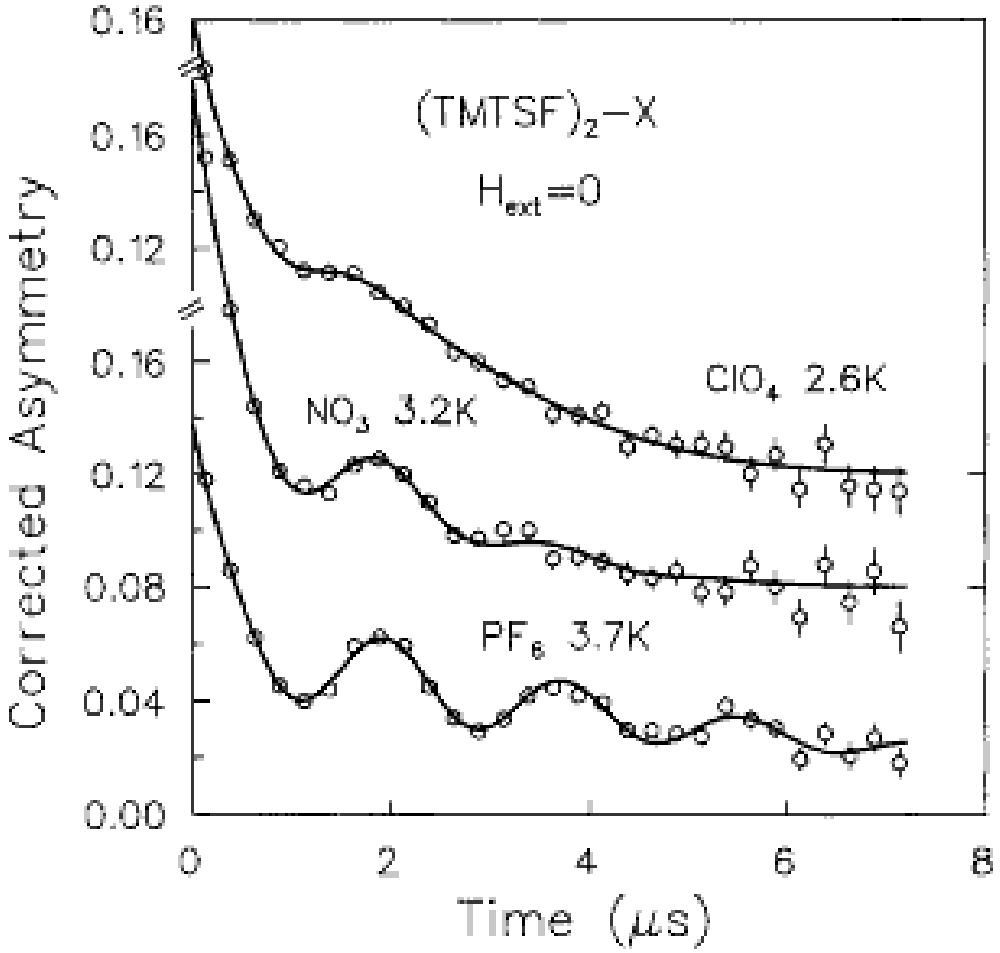

L.P. Le et al, PRB **48** 7284 (1993)

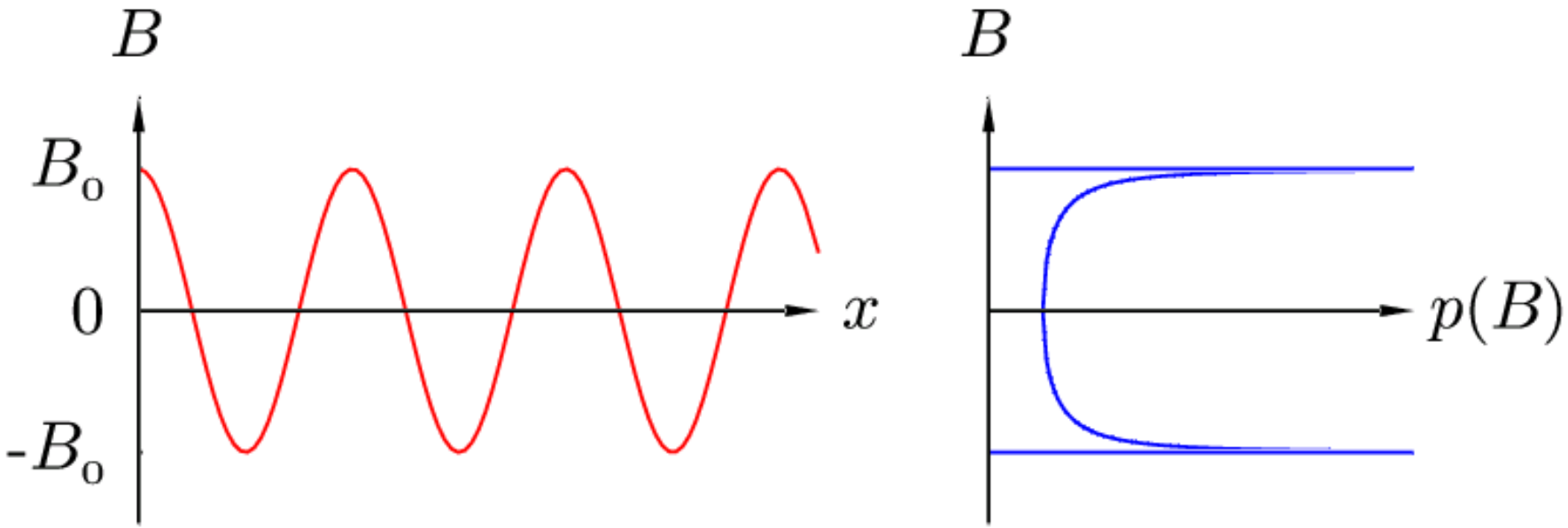

$$B = B_0 \cos(x) \implies p(B) = (2/\pi)(B_0^2 - B^2)^{-1/2}$$

$$A(t) = \int_{-B_0}^{B_0} p(B) \cos(\gamma_\mu B t)\, dB = J_o(\gamma_\mu B_0 t)$$

$J_0(\xi) \to (2/\pi\xi)^{1/2} \cos(\xi - \pi/4)$ as $\xi \gg 1$
$A(t)$ has turning points when $\gamma_\mu B_o t \sim (n + 1/4)\pi$

SDW phase in $(TMTSF)_2X$

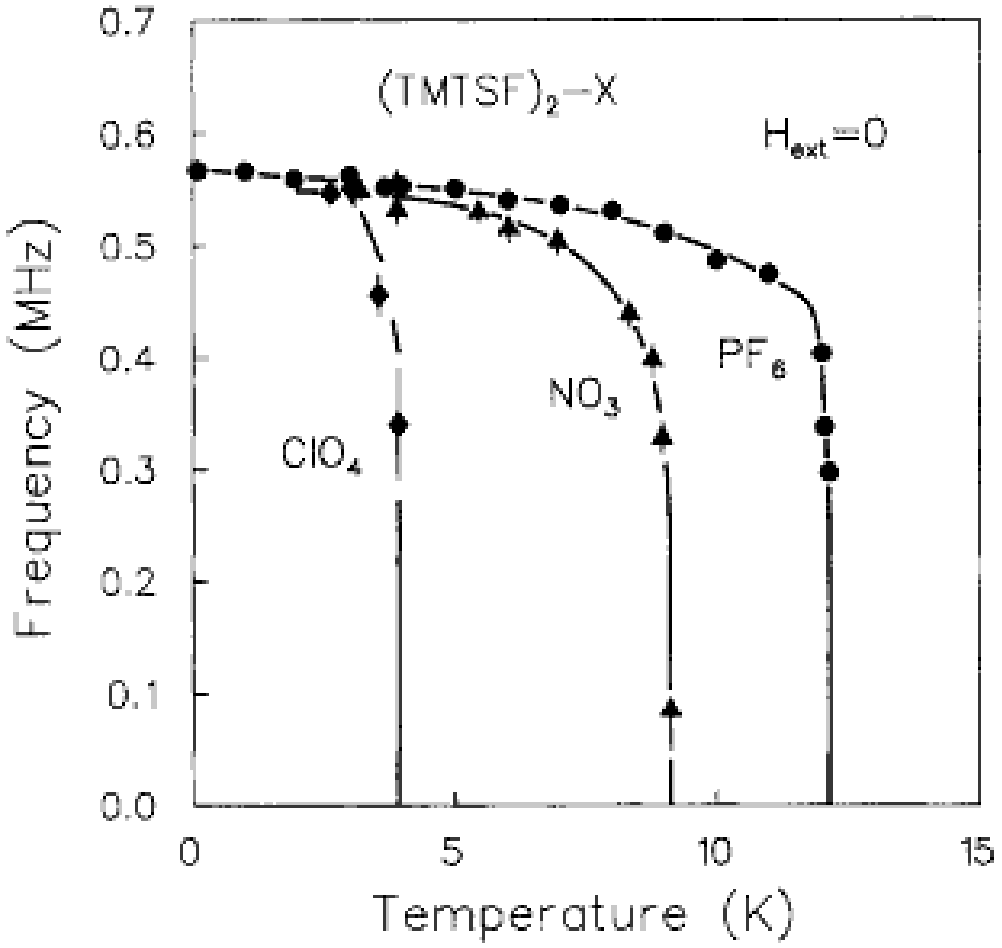

L.P. Le et al, PRB **48** 7284 (1993)

Muon-spin relaxation

$$P_z(t) = P_z(0)\, e^{-\Gamma t}$$

Muon polarization

Relaxation rate

$$\Gamma = \int_0^\infty \gamma_\mu^2 \langle B_\perp(t)\, B_\perp(0) \rangle \cos \omega_L t \; dt$$

Field-field correlation function

$\gamma_\mu B_L$

longitudinal field

$2(\Delta/\gamma_\mu)^2$

If $\langle B_\perp(t) B_\perp(0) \rangle = \langle B_\perp^2 \rangle e^{-\nu t}$

ν: field-field correlation rate

$$\Rightarrow \quad \Gamma = \frac{2\Delta^2 \nu}{\nu^2 + \omega_L^2}$$

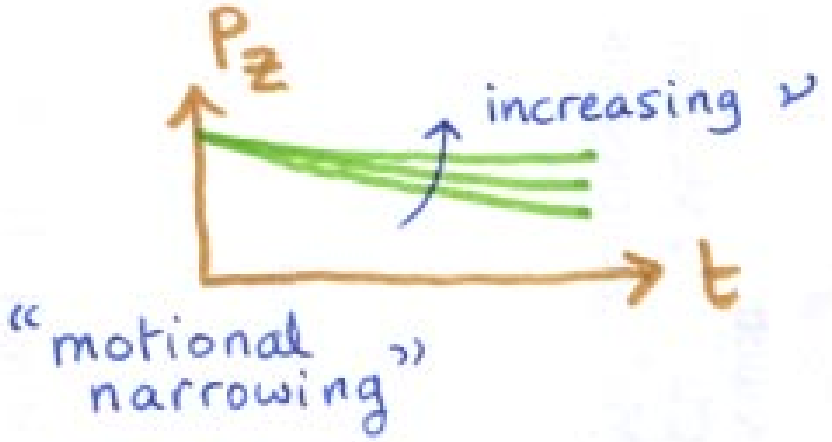

- $\omega_L = 0 \qquad \Gamma = 2\Delta^2/\nu$

- $\omega_L \neq 0 \qquad \Gamma \to 0 \quad$ as $\quad \frac{\omega_L}{\nu} \to \infty$

Relaxation functions

Static distribution of local fields

"Kubo-Toyabe" relaxation function

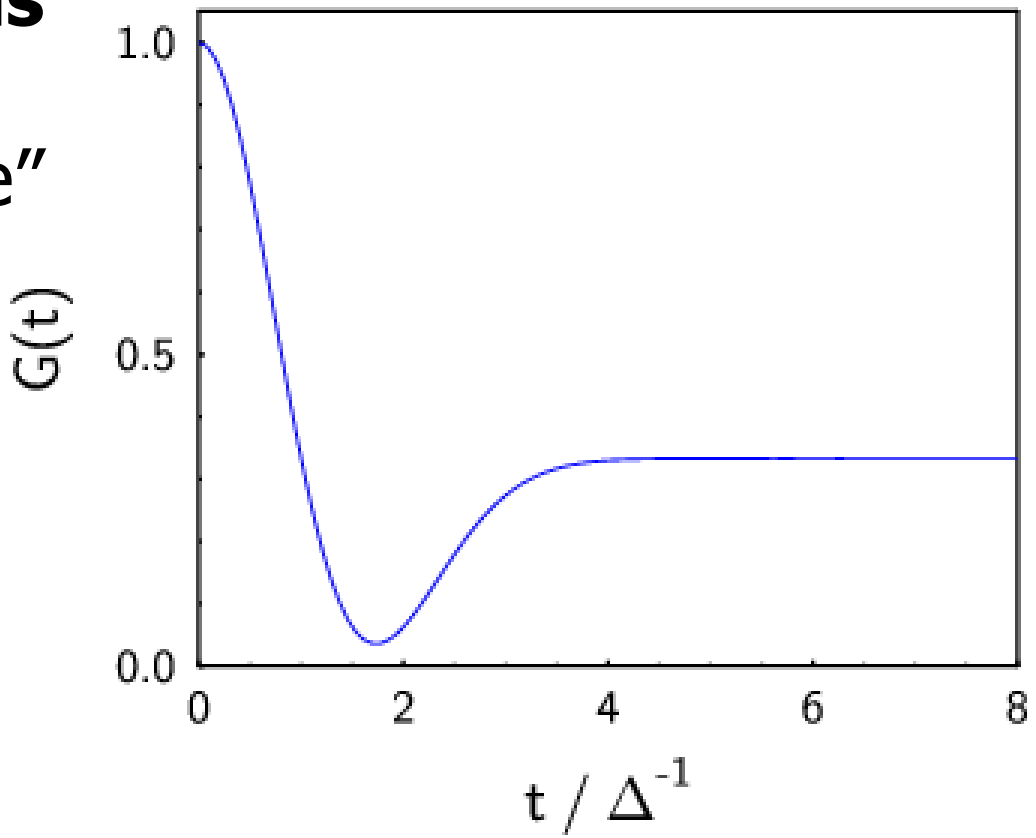

Relaxation functions

Static distribution of local fields

"Kubo-Toyabe" relaxation function

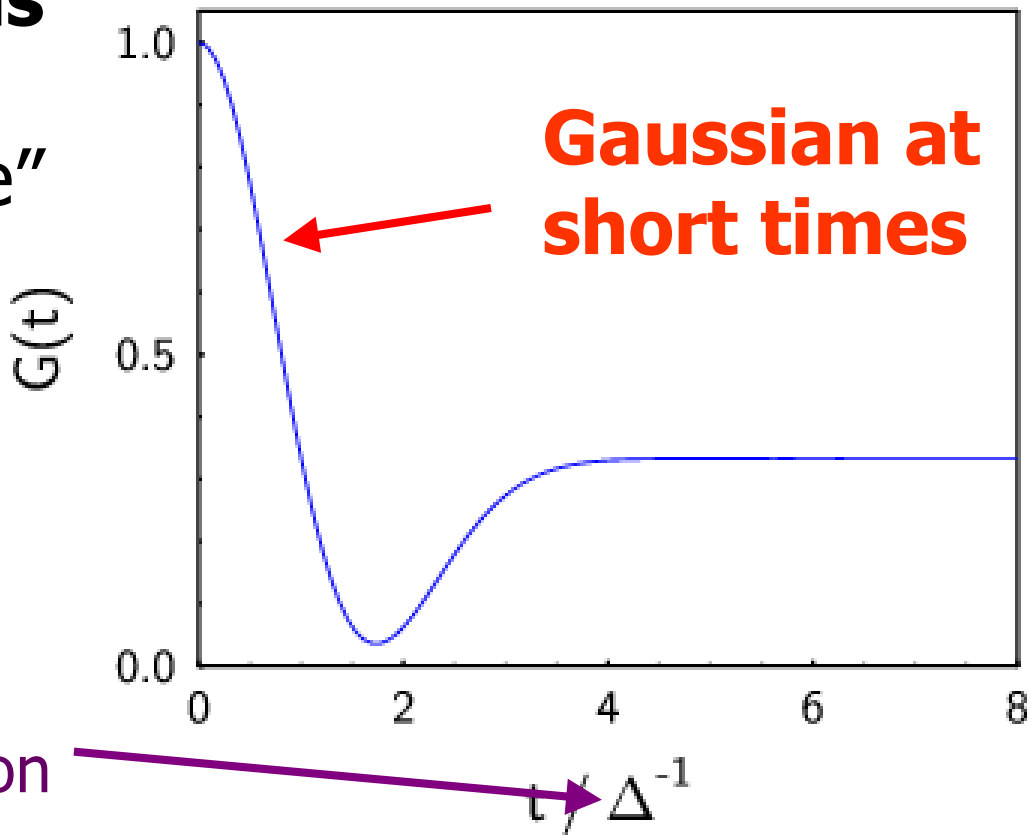

Δ is the width of the static distribution

Relaxation functions

Dynamical fluctuations

exponential relaxation function

Fluctuation rate: ν

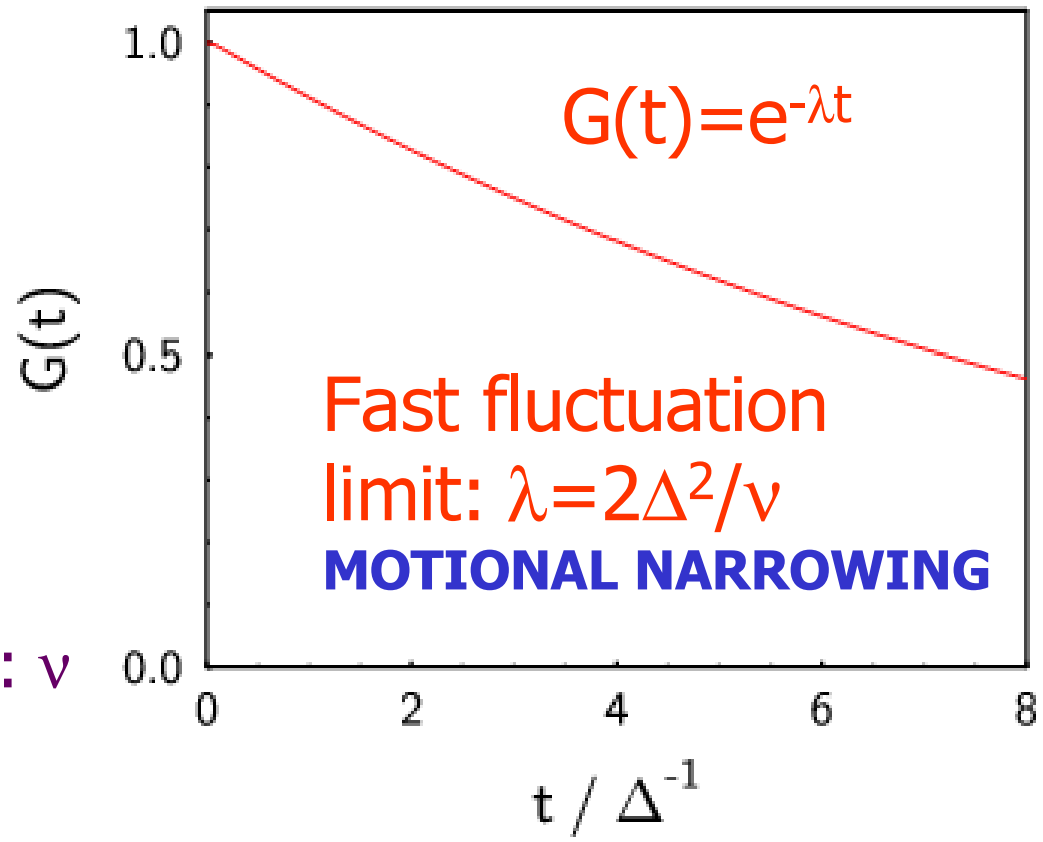

Relaxation functions

One can interpolate between statics and dynamics using a **dynamical Kubo-Toyabe function**

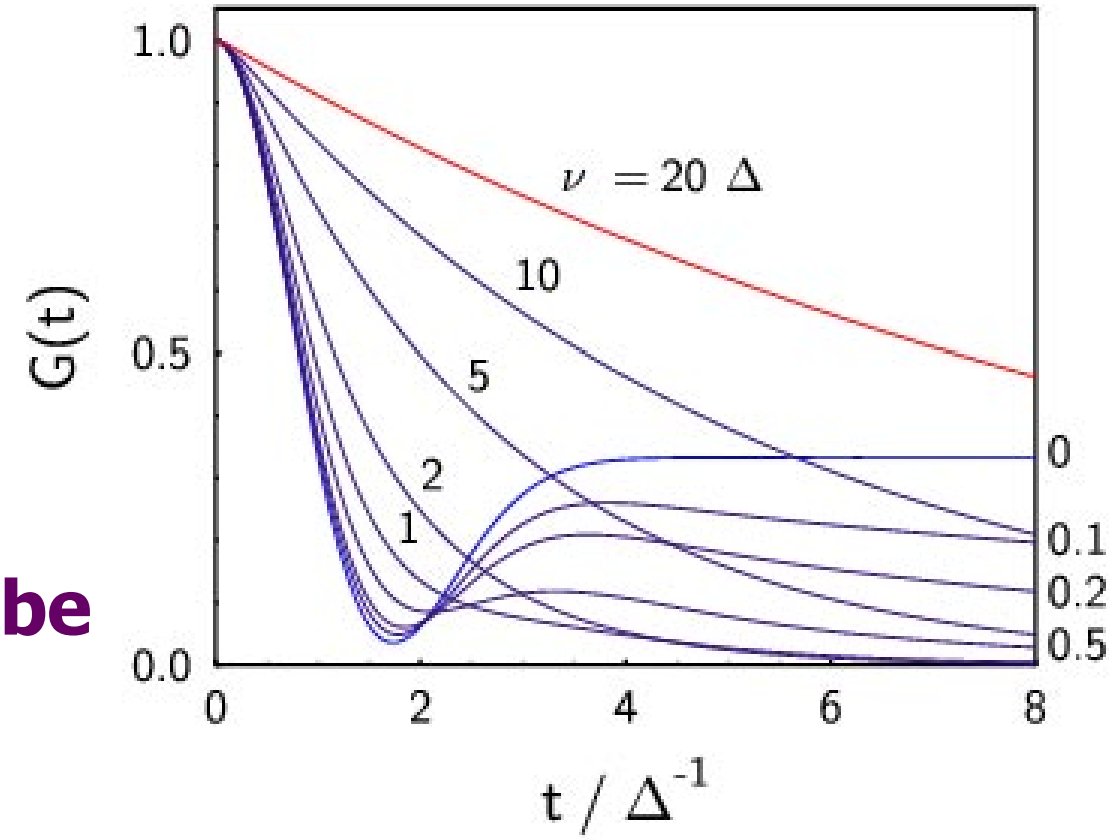

Muons and spin glasses

Muons that stop closer to magnetic ions "see" a wider local field distribution (which extends to higher fields) than muons which stop at a greater distance

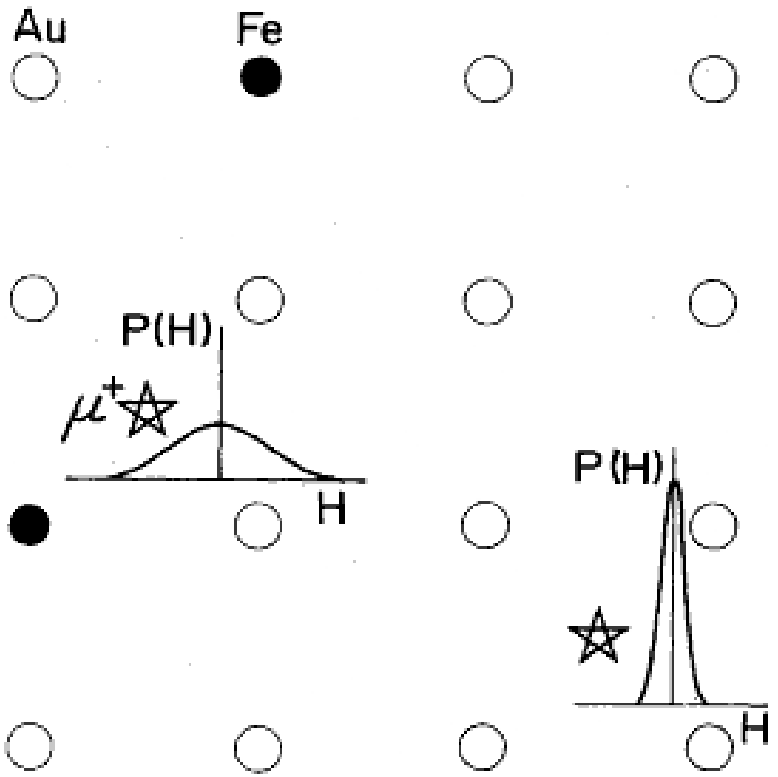

FIG. 3. Schematic view of different variable ranges of random local fields at different muon sites in dilute-alloy spin glasses. When Fe (or Mn) moments fluctuate, the local field at muon sites closer to the magnetic ions will be modulated in a wider range.

Y.J. Uemura et al,
PRB **31**, 546 (1985)

Range of coupling strengths

i.e. distribution of Δ

PRB 31 546 '85
PRB 50 10039 '94

$$\rho(\Delta) = \sqrt{\frac{2}{\pi}}\,\frac{a}{\Delta^2}\,e^{-a^2/2\Delta^2}$$

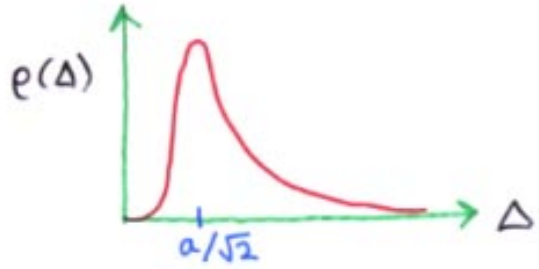

$\langle\Delta\rangle \sim a$

so that

$$P(t) = \int_0^\infty e^{-\Gamma t}\,\rho(\Delta)\,d\Delta$$

$$= \exp\left[-(\lambda t)^{1/2}\right]$$

where

$$\lambda = \frac{2a^2\Gamma}{\Delta^2} = \frac{4a^2\nu}{\omega_L^2 + \nu^2}$$

so that $\lambda^{-1} = A_1 + A_2 B_L^2$

A_1, A_2: constants

deduce ν, a

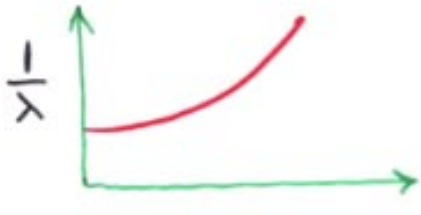

Stretched exponential

$$G(t)=G(0)\exp(-(\lambda t)^{\beta})$$

- $\beta=2$ (Gaussian) static nuclear dipoles, observable if electronic moment dynamics too fast (motional narrowing)
- $\beta=1$ (exponential) dynamics
- $\beta=0.5$ (root-exponential) dilute-spins and dynamics

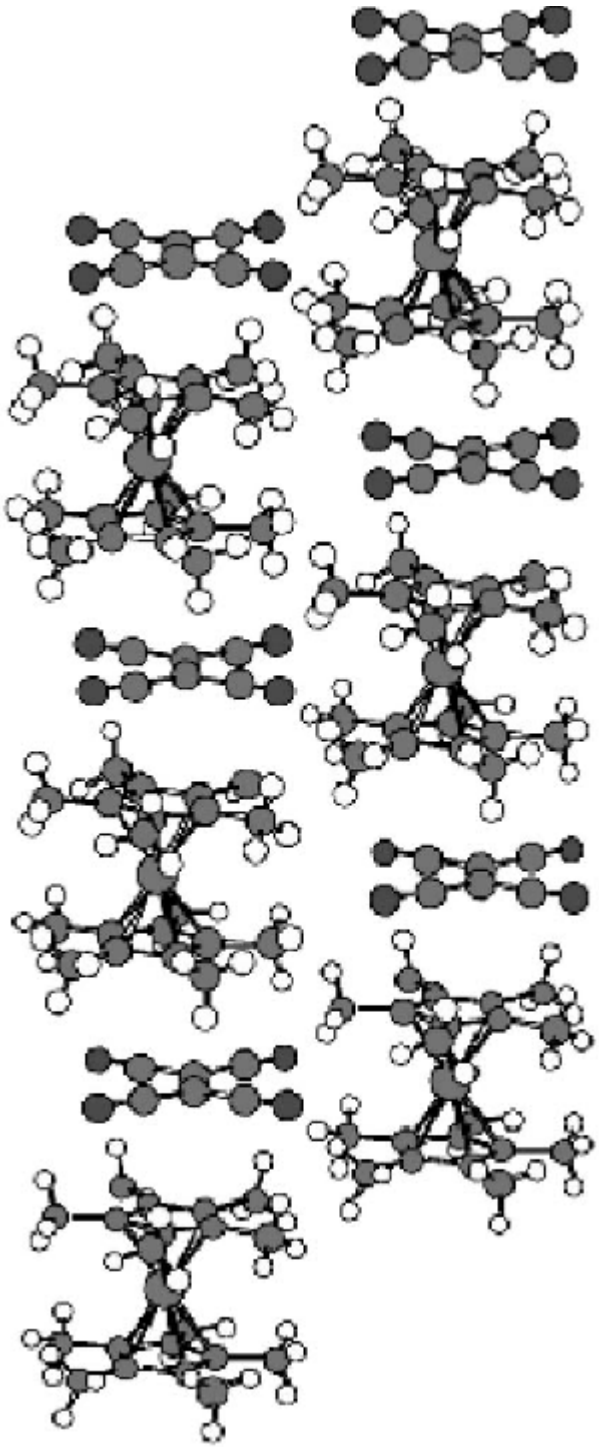

TCNE

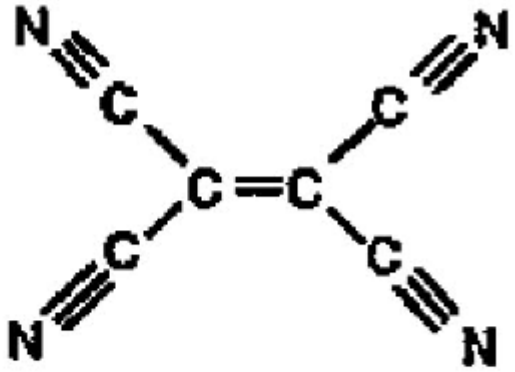

$[Fe(C_5Me_5)_2]$

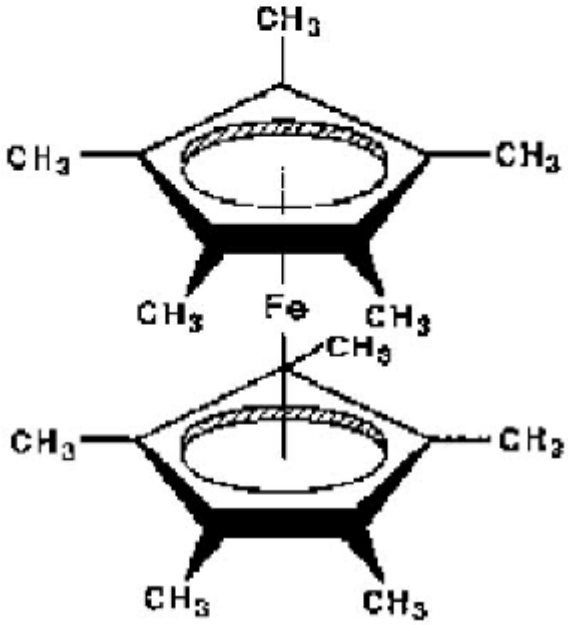

(DMeFc)(TCNE)

1D molecular ferromagnet

T_c=5 K

* at low temperature data observe Kubo Toyabe relaxation function (broad internal field distribution)

* above T_c, see dynamic behaviour corresponding to spin fluctuations

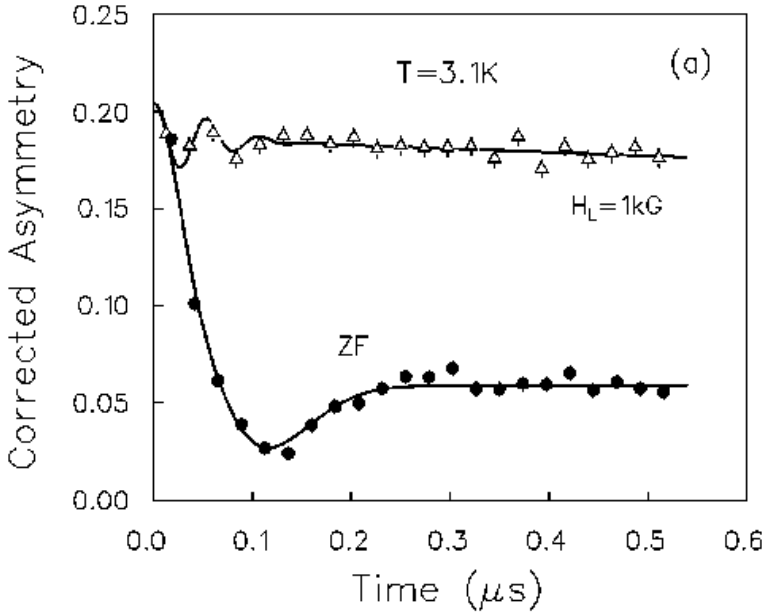

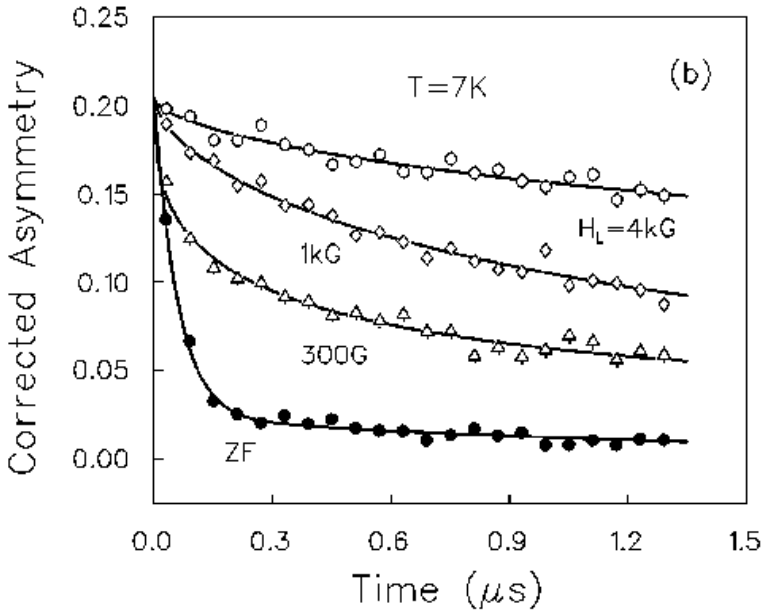

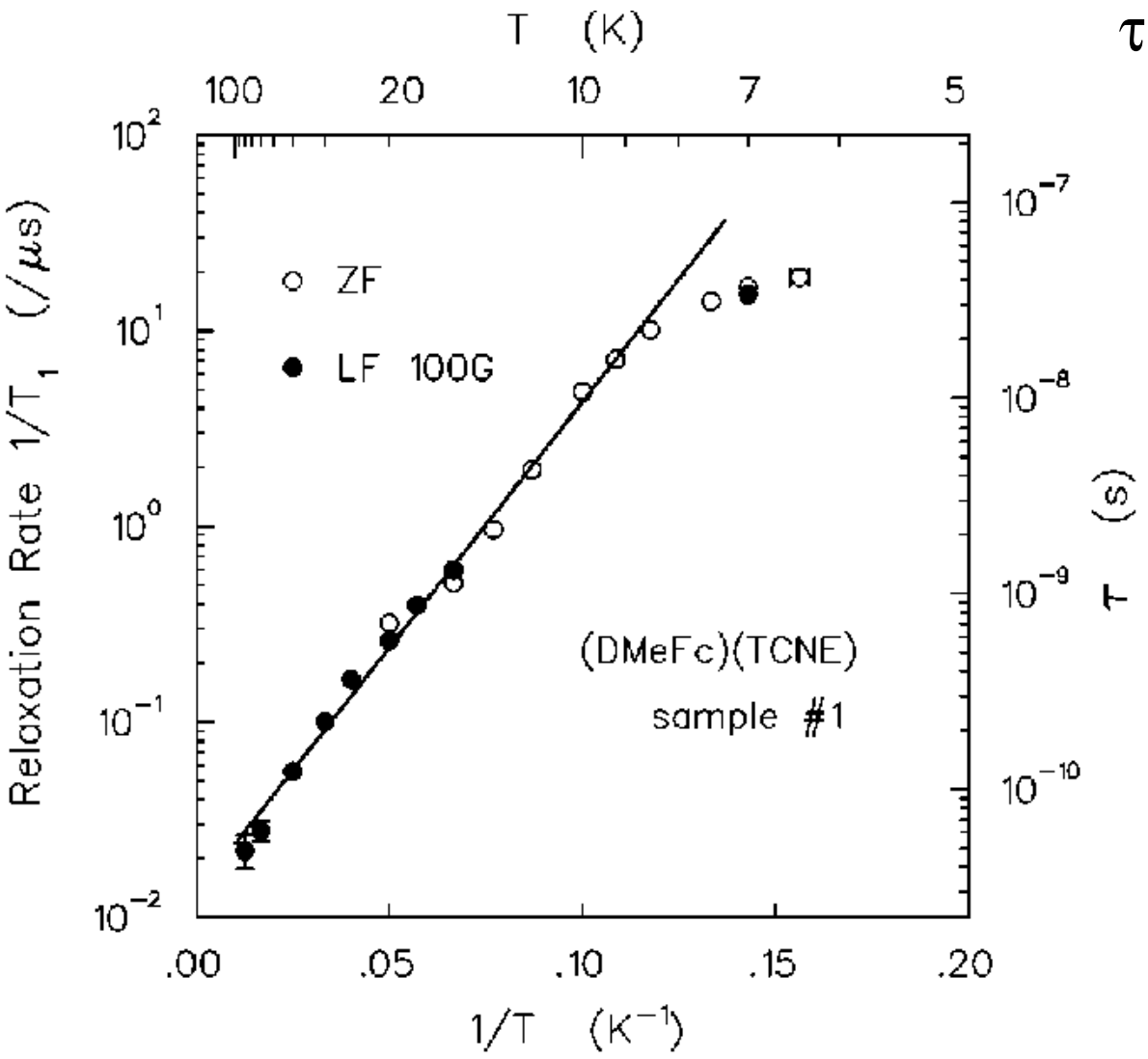

$\tau(T) = \tau_\infty \exp(E_a/k_B T)$

$E_a/k_B = 57.8 \sim 2J$

$\tau_\infty >> h/J$

Ising chain

L.P. Le et al PRB **65** 024432 (2002)

Fe_{19}-etheidi

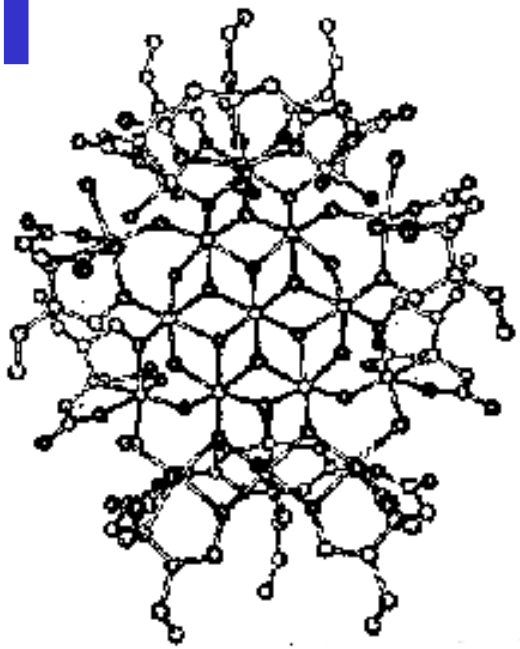

Magnetic nanodiscs

disc-shaped molecules
forms well defined stacks

S = 33/2 [!!]

chemical formula: $[Fe_{19}(etheidi)_{10}(OH)_{14}O_6(H_2O)_{12}]NO_3 \cdot 18H_20$

"highly engineered rust"

J.C. Goodwin et al, J Chem. Soc. Dalton Trans. 1835 (2000)

(orders antiferromagnetically at 1.07 K, see M. Affronte et al, PRB **66** 064408 (2002))

Raw muon data:

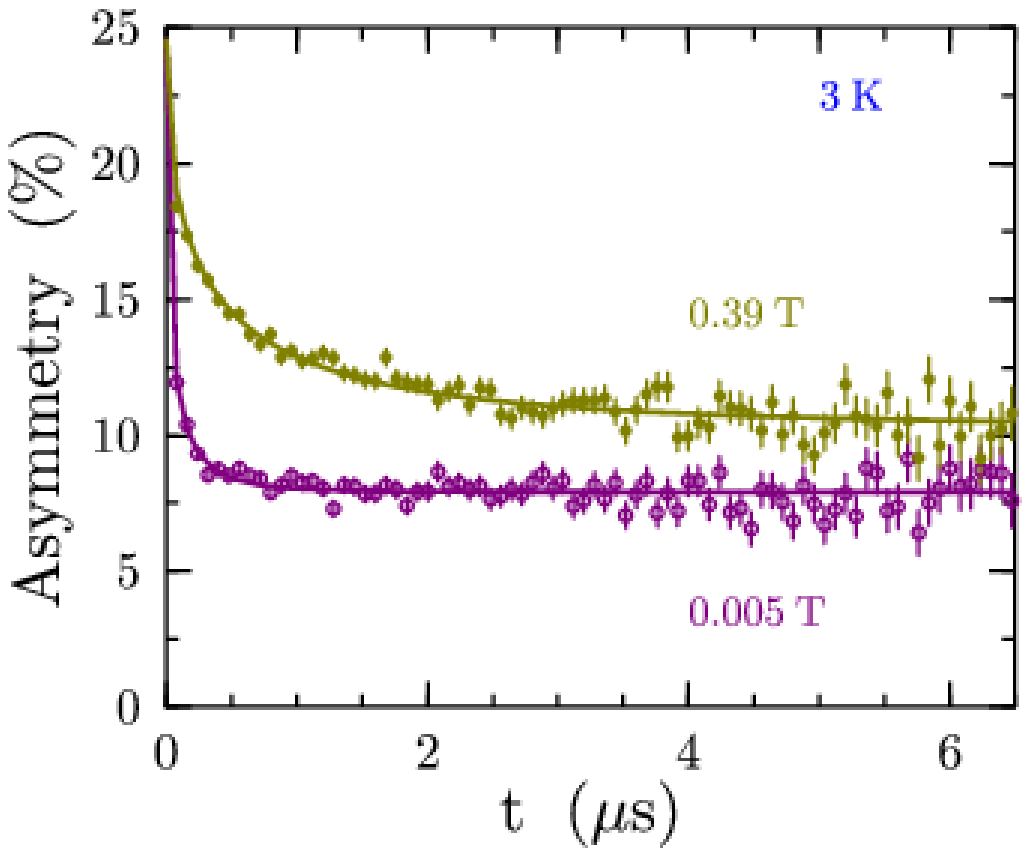

Very fast relaxation which is not quenched with the application of 0.39 T. $\Rightarrow$ spins are dynamically fluctuating

Root exponential form fits all data
(see Salman et al. PRB 65 132403 (2002), Keren PRB 50 10039 (1994)).

Field dependence of muon relaxation rate in Fe_{19}-etheidi

Activated
at high
temperature

Constant at
low temperature

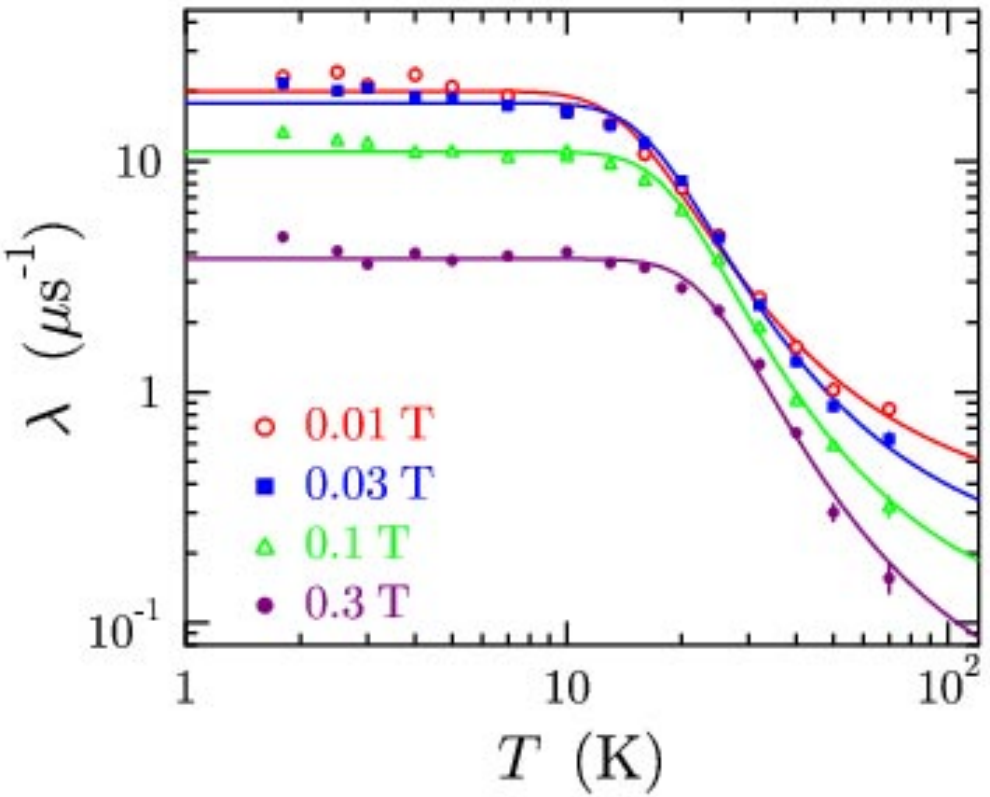

$\lambda=(\lambda_H^{-1}+e^{-U/T})^{-1}$ where λ_H is the low temperature field-dependent relaxation

S.J. Blundell et al in press.

Low temperature relaxation rate

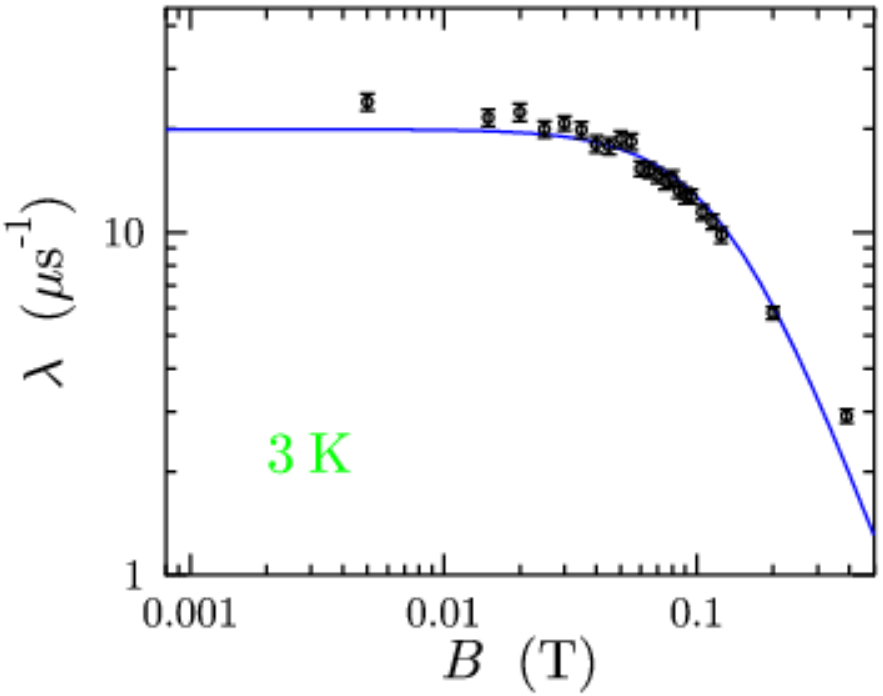

$\lambda_H^{-1}=A_1+A_2B^2$ where $A_1=\nu/(2\gamma_\mu^2a^2)$, $A_2 = 1/(2\nu a^2)$

$\Rightarrow$ quantum tunneling rate can be extracted.

S.J. Blundell et al in press.

Peierls distortion

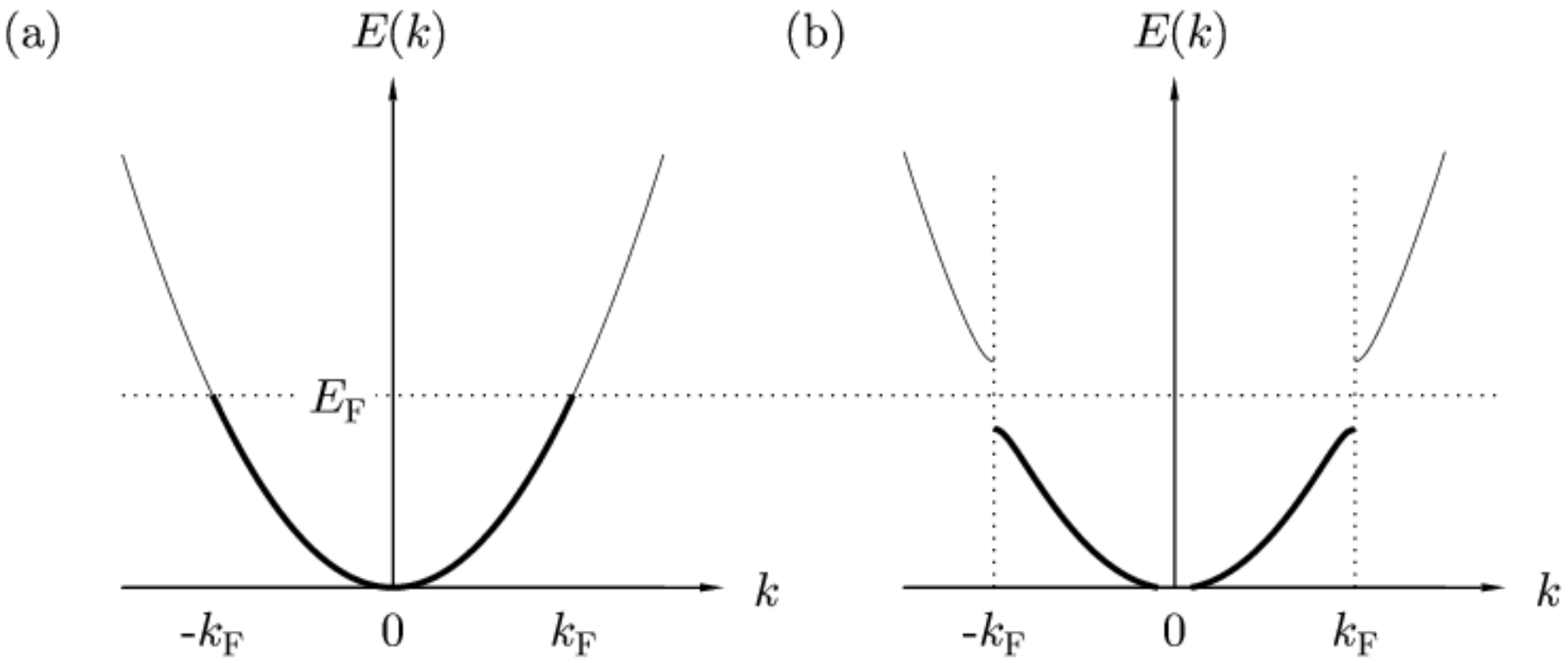

Elastic energy cost outweighed by electronic gain below a critical temperature $T_p \sim (E_F/k_B) \exp(-1/\lambda_{electron\text{-}phonon})$

Spin-Peierls distortion

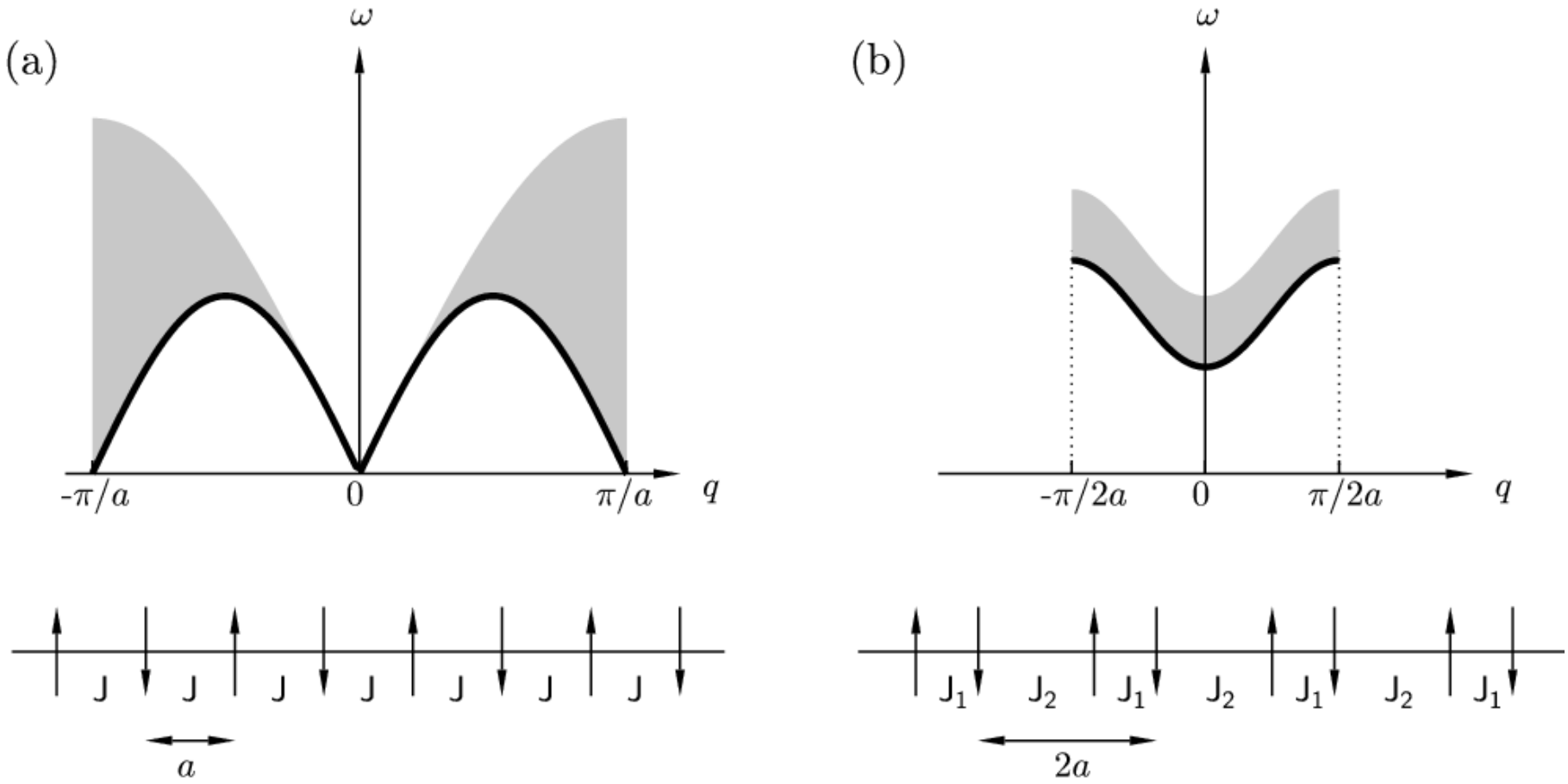

Elastic energy cost outweighed by magnetic gain below a critical temperature $T_{sp} \sim (E_F/k_B) \exp(-1/\lambda_{spin\text{-}phonon})$

(a) MEM$^+$ (b) TCNQ

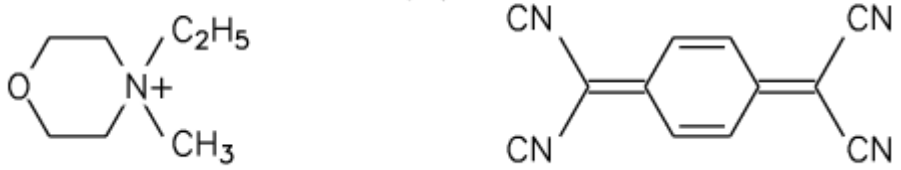

MEM(TCNQ)$_2$

T_{sp} = 18 K

(actually T_p = 335 K)

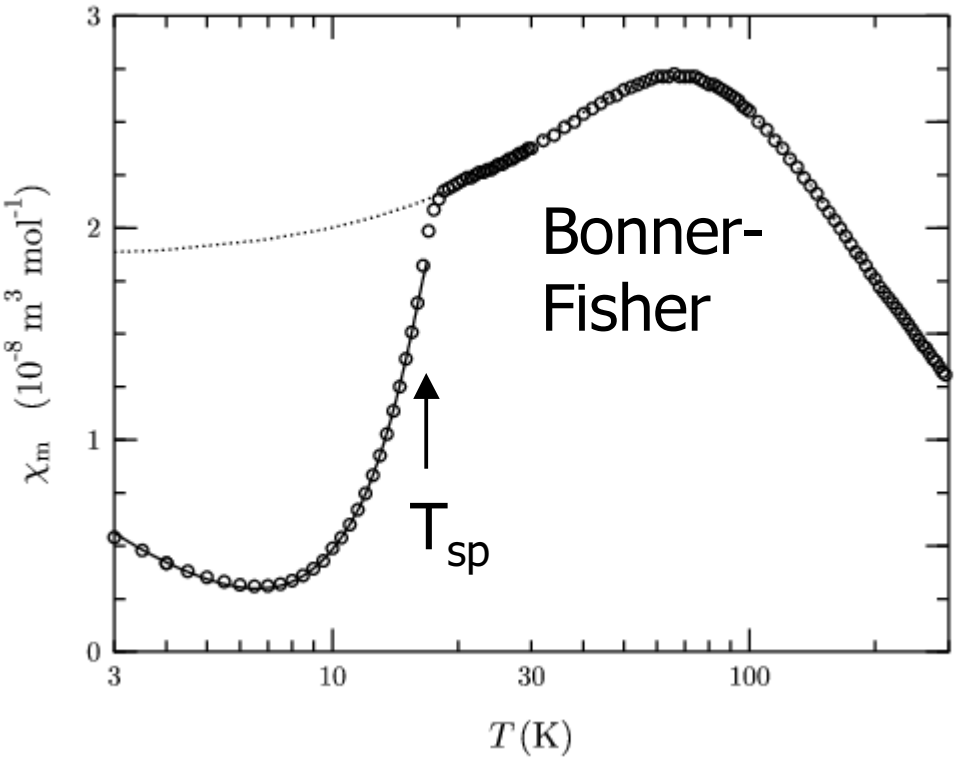

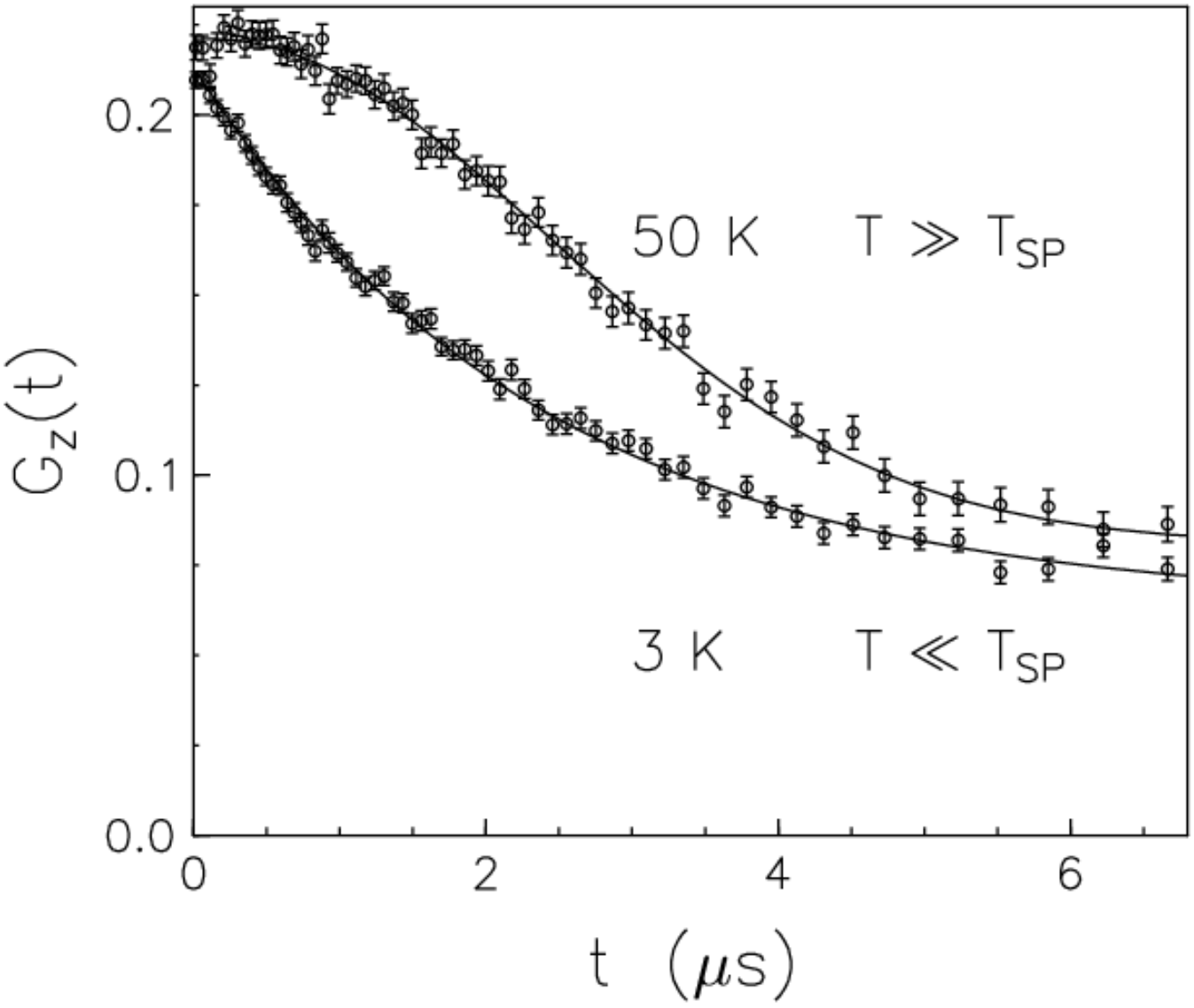

SJB et al. J. Phys.: Condens. Matter 9, L119 (1997)

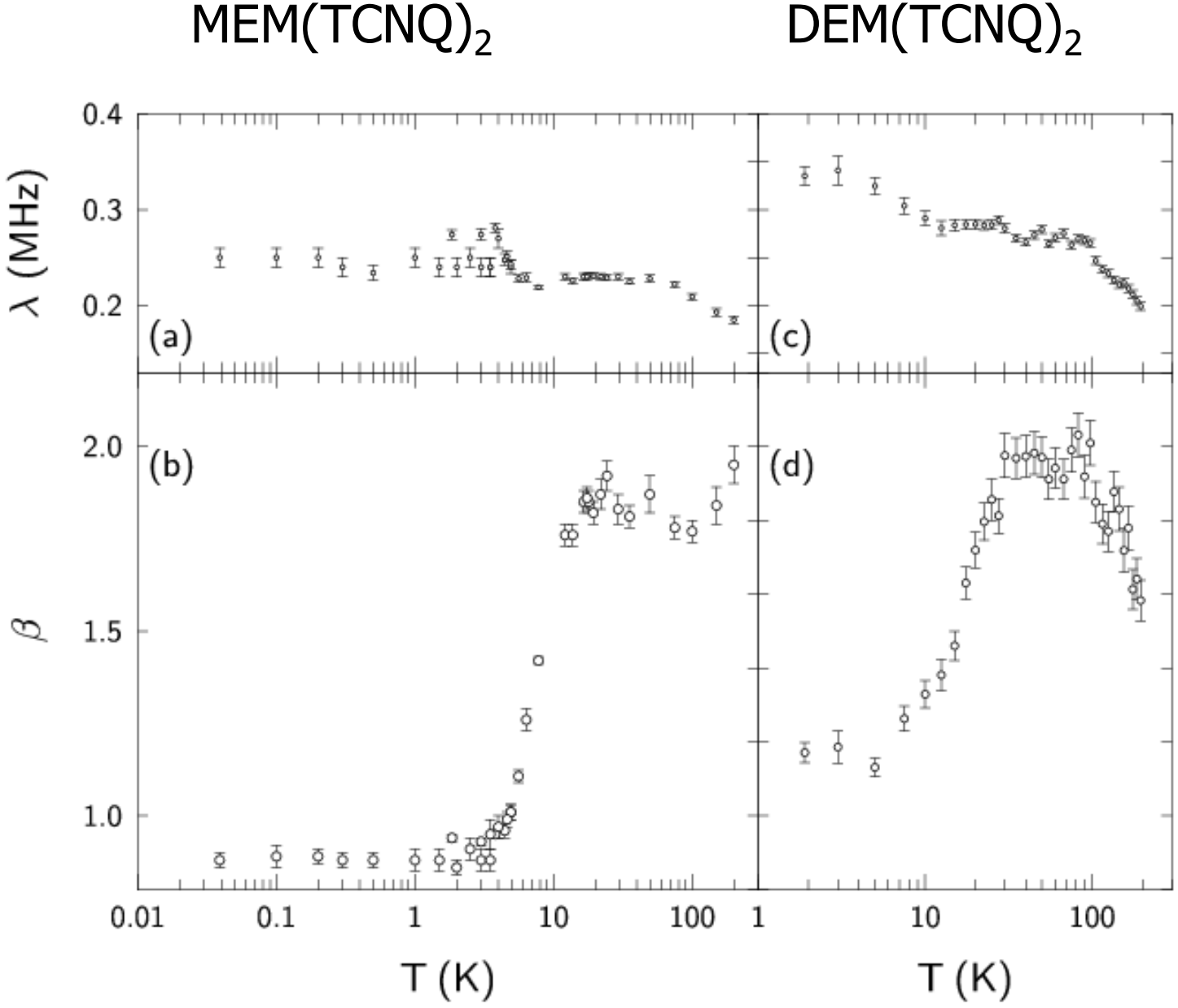
MEM(TCNQ)2
DEM(TCNQ)2
λ (MHz)
β
(a)
(b)
(c)
(d)
0.4
0.3
0.2
2.0
1.5
1.0
0.01
0.1
1
10
100
1
10
100
T (K)
T (K)

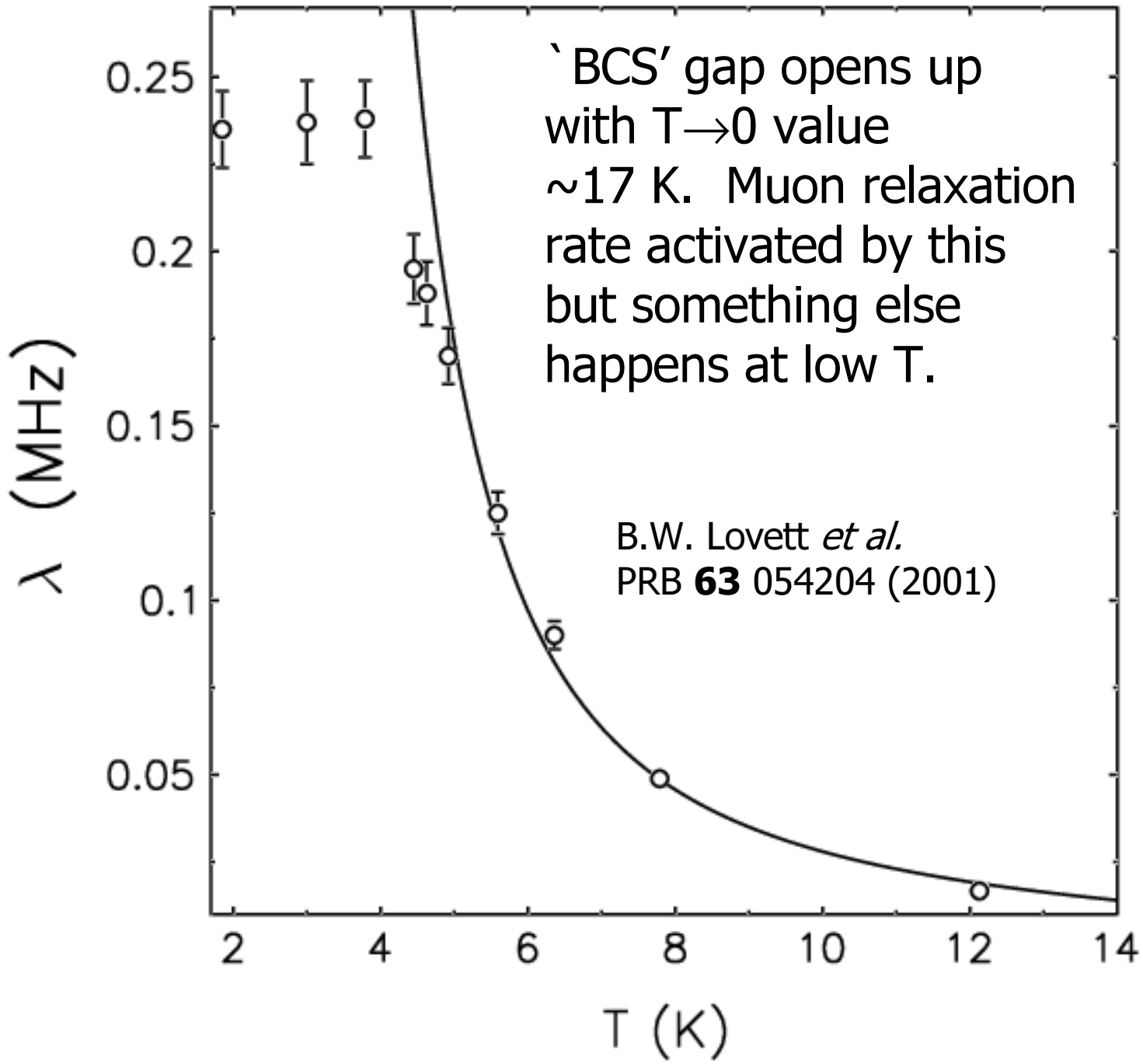
`BCS' gap opens up with T→0 value ~17 K. Muon relaxation rate activated by this but something else happens at low T.
B.W. Lovett *et al.*
PRB **63** 054204 (2001)
λ (MHz)
T (K)
0.25
0.2
0.15
0.1
0.05
2
4
6
8
10
12
14

That's all folks!